NATURAL RESOURCES

ANALYTICAL DATA FROM THE HOODSPORT 7.5-MINUTE QUADRANGLE, MASON COUNTY, WASHINGTON—SUPPLEMENT TO OPEN FILE REPORT 2011-3

by Michael Polenz, Brendan A. Miller,
Nigel Davies, Benjamin B. Perry,
Jonathan F. Hughes, Kenneth P. Clark,
Timothy J. Walsh, Jeffrey H. Tepper,
and Robert J. Carson

WASHINGTON
DIVISION OF GEOLOGY
AND EARTH RESOURCES
Open File Report 2011-4
August 2012

WASHINGTON STATE DEPARTMENT OF
Natural Resources
Peter Goldmark - Commissioner of Public Lands

ANALYTICAL DATA FROM THE HOODSPORT 7.5-MINUTE QUADRANGLE, MASON COUNTY, WASHINGTON—SUPPLEMENT TO OPEN FILE REPORT 2011-3

by Michael Polenz, Brendan A. Miller,
Nigel Davies, Benjamin B. Perry,
Jonathan F. Hughes, Kenneth P. Clark,
Timothy J. Walsh, Jeffrey H. Tepper,
and Robert J. Carson

WASHINGTON
DIVISION OF GEOLOGY
AND EARTH RESOURCES
Open File Report 2011-4
August 2012

WASHINGTON STATE DEPARTMENT OF
Natural Resources
Peter Goldmark - Commissioner of Public Lands

DISCLAIMER
Neither the State of Washington, nor any agency thereof, nor any of their employees, makes any warranty, express or implied, or assumes any legal liability or responsibility for the accuracy, completeness, or usefulness of any information, apparatus, product, or process disclosed, or represents that its use would not infringe privately owned rights. Reference herein to any specific commercial product, process, or service by trade name, trademark, manufacturer, or otherwise, does not necessarily constitute or imply its endorsement, recommendation, or favoring by the State of Washington or any agency thereof. The views and opinions of authors expressed herein do not necessarily state or reflect those of the State of Washington or any agency thereof.

WASHINGTON STATE DEPARTMENT OF NATURAL RESOURCES
Peter Goldmark—*Commissioner of Public Lands*

DIVISION OF GEOLOGY AND EARTH RESOURCES
David K. Norman—*State Geologist*
John P. Bromley—*Assistant State Geologist*

Washington State Department of Natural Resources
Division of Geology and Earth Resources

Mailing Address:
MS 47007
Olympia, WA 98504-7007

Street Address:
Natural Resources Bldg, Rm 148
1111 Washington St SE
Olympia, WA 98501

Phone: 360-902-1450
Fax: 360-902-1785
E-mail: geology@dnr.wa.gov
Website: http://www.dnr.wa.gov/ResearchScience/GeologyEarthSciences/Pages/Home.aspx

Publications List:
http://www.dnr.wa.gov/ResearchScience/Topics/GeologyPublicationsLibrary/Pages/pubs.aspx

Washington Geology Library Catalog:
http://www.dnr.wa.gov/ResearchScience/Topics/GeologyPublicationsLibrary/Pages/washbib.aspx

Washington State Geologic Information Portal:
http://www.dnr.wa.gov/ResearchScience/Topics/GeosciencesData/Pages/geology_portal.aspx

Suggested Citation: Polenz, Michael; Miller, B. A.; Davies, Nigel; Perry, B. B.; Hughes, J. F.; Clark, K. P.; Walsh, T. J.; Tepper, J. H.; Carson, R. J., 2012, Analytical data from the Hoodsport 7.5-minute quadrangle, Mason County, Washington—Supplement to Open File Report 2011-3: Washington Division of Geology and Earth Resources Open File Report 2011-4, 42 p.

Published in the United States of America
© 2012 Washington Division of Geology and Earth Resources

Table of Contents

Geologic Setting....1
Bedrock Characterization....1
Eocene Volcanic and Sedimentary Rocks of the Crescent Formation....1
Sedimentary Rocks Above the Crescent Formation....3
Bedrock Types from Which Quaternary Deposits Are Derived....3
Quaternary Deposits....6
Quaternary Stratigraphy....6
Age-Control Data....7
Timing and Duration of Vashon Ice in the Hoodsport Quadrangle....8
Fraser(?) Olympic Ice in the Map Area....12
Shores of Ice-dammed Lake(s?) along Hood Canal....12
Structure....15
Tectonic Setting....15
Evidence for Post-Glacial Tectonic Effects....17
Mapped Faults and Folds....17
Saddle Mountain Fault Zone....17
Post-glacial Tectonic Effects....20
Saddle Mountain East Fault....21
Saddle Mountain West Fault....21
Dow Mountain Fault....22
Frigid Creek Fault....24
Unnamed Fault East of the Saddle Mountain East Fault....26
Other Unnamed Faults....26
Miller Creek Syncline....26
Other Structures....28
Lucky Dog Structure....28
Hood Canal Fault....28
Acknowledgments....29
References Cited....29

Appendix A. Age-control data....34

Figures

Figure 1. Lidar hillshade showing geomagnetic field-strength anomalies and pole-rotated, abrupt field-strength boundaries....2
Figure 2. Photo of Douglas-fir stump top at the western edge of Price Lake....8
Figure 3. Photo and analysis of tephra found beneath a wetland on the southern edge of Price Lake....9
Figure 4a. Photo of Vashon advance glaciolacustrine sediment at age location UFCVA of Polenz and others (2012)....10

Figure 4b. Photo of conifer needles in laminated to massive glaciolacustrine mud at age location UFCVA 11
Figure 5. Lidar hillshade showing east-southeast-trending fabric in the surface morphology of the western half of a lumpy hill east of Lake Cushman 12
Figure 6. Graph showing regional glacio-isostatic rebound tilt slope and glaciolacustrine shoreline markers along southern Hood Canal 15
Figure 7. Photo of the view south from Saddle Mountain across Price Lake to Dow Mountain 18
Figure 8. Lidar hillshade showing mapped strands of the Saddle Mountain fault zone in north-central portion of the Hoodsport quadrangle 19
Figure 9. Photo showing Crescent Formation basalt with multiple shear planes interpreted as likely Saddle Mountain East fault strand exposures 22
Figure 10. Photo showing view to southeast of the Dow Mountain fault 23
Figure 11. Photo showing an east-northeast view of Frigid Creek fault investigation trench exposure 1,500 ft west of the map area 24
Figure 12. Photo of the view to southwest of "Alligator trench" exposing the unnamed fault east of the Saddle Mountain East fault 25
Figure 13a. Photo of the view to southwest of southeast-dipping rhythmite beds of unit ΦEm northwest of the Miller Creek syncline 27
Figure 13b. Close-up photo of southeast-dipping rhythmite beds of unit ΦEm 27
Figure 13c. Photo of gently undulating, nearly horizontal rhythmite beds of unit ΦEm in southeast limb of Miller Creek syncline 27

Tables

Table 1. Geochemical analyses of volcanic bedrock samples from the Hoodsport quadrangle 4
Table 2. Glacial lake delta elevation estimates in the Hoodsport and Skokomish Valley quadrangles 14

Analytical Data from the Hoodsport 7.5-minute Quadrangle, Mason County, Washington—Supplement to Open File Report 2011-3

Michael Polenz[1], Brendan A. Miller[2], Nigel Davies[1], Benjamin B. Perry[1], Jonathan F. Hughes[3], Kenneth P. Clark[4], Timothy J. Walsh[1], Jeffrey H. Tepper[4], Robert J. Carson[5]

[1] Washington Division of Geology and Earth Resources
MS Box 47007
Olympia, WA 98504-7007

[2] Department of Earth and Space Sciences
University of Washington
Johnson Hall, Room 070, Box 351310
4000 15th Ave NE
Seattle, WA 98195-1310

[3] Department of Geography
University of the Fraser Valley
33844 King Road
Abbotsford, BC V2S 7M8
Canada

[4] Geology Department
University of Puget Sound
1500 N Warner
Tacoma, WA 98416

[5] Department of Geology
Whitman College
Walla Walla, WA 99362

GEOLOGIC SETTING

The Hoodsport quadrangle in the southeastern Olympic Mountains of Washington is situated in the Paleocene to Eocene Coast Range Volcanic Province (Hirsch and Babcock, 2009) along the Cascadia forearc. The quadrangle is bounded to the east by the fjord-like Hood Canal and the repeatedly glaciated Puget Lowland. The landforms and rocks in the quadrangle are defined by the interaction of the bedrock of the southeastern Olympic Mountains with repeated incursions of glacial ice from the Olympic Mountains and the Cordilleran continental ice sheet.

Bedrock Characterization

EOCENE VOLCANIC AND SEDIMENTARY ROCKS OF THE CRESCENT FORMATION

Volcanic bedrock in the quadrangle has previously been mapped as Eocene Crescent Formation basalt flows, pillows, breccias, and mudflow breccias, with sedimentary interbeds (Wilson, 1975; Carson, 1976; Tabor and Cady, 1978; Logan, 2003). We have made no attempt to separately map the “upper” and “lower” members of the Crescent Formation. However, based on prior mapping (Tabor and Cady, 1978), abundance of brecciated basalt exposures in the Hoodsport quadrangle, consultation with Rowland Tabor and Richard Blakely (both U.S. Geological Survey [USGS], written commun., 2010 and 2011), and in consideration of inconclusive chemical trends, we speculate that a northeast-trending geomagnetic boundary (Fig. 1) across the northwest corner of the quadrangle (see Polenz and others, 2012) may mark the boundary between the upper and lower members of the formation, such that nearly all Crescent Formation exposures in the quadrangle should be associated with the upper member. A magnetic susceptibility image that is filtered to emphasize shallow magnetic sources (not shown; Blakely, written commun., 2011) would show this geomagnetic boundary as more abrupt transition than the rainbow-colored backdrop to Figure 1. However, a reasonable alternative interpretation (Blakely, written commun., 2011) would place the boundary along a strand of the Saddle Mountain fault zone (black northeast-trending line across lower right of Fig. 1) 2.5 mi southeast of the above-proposed boundary, which also coincides with a strong geomagnetic boundary.

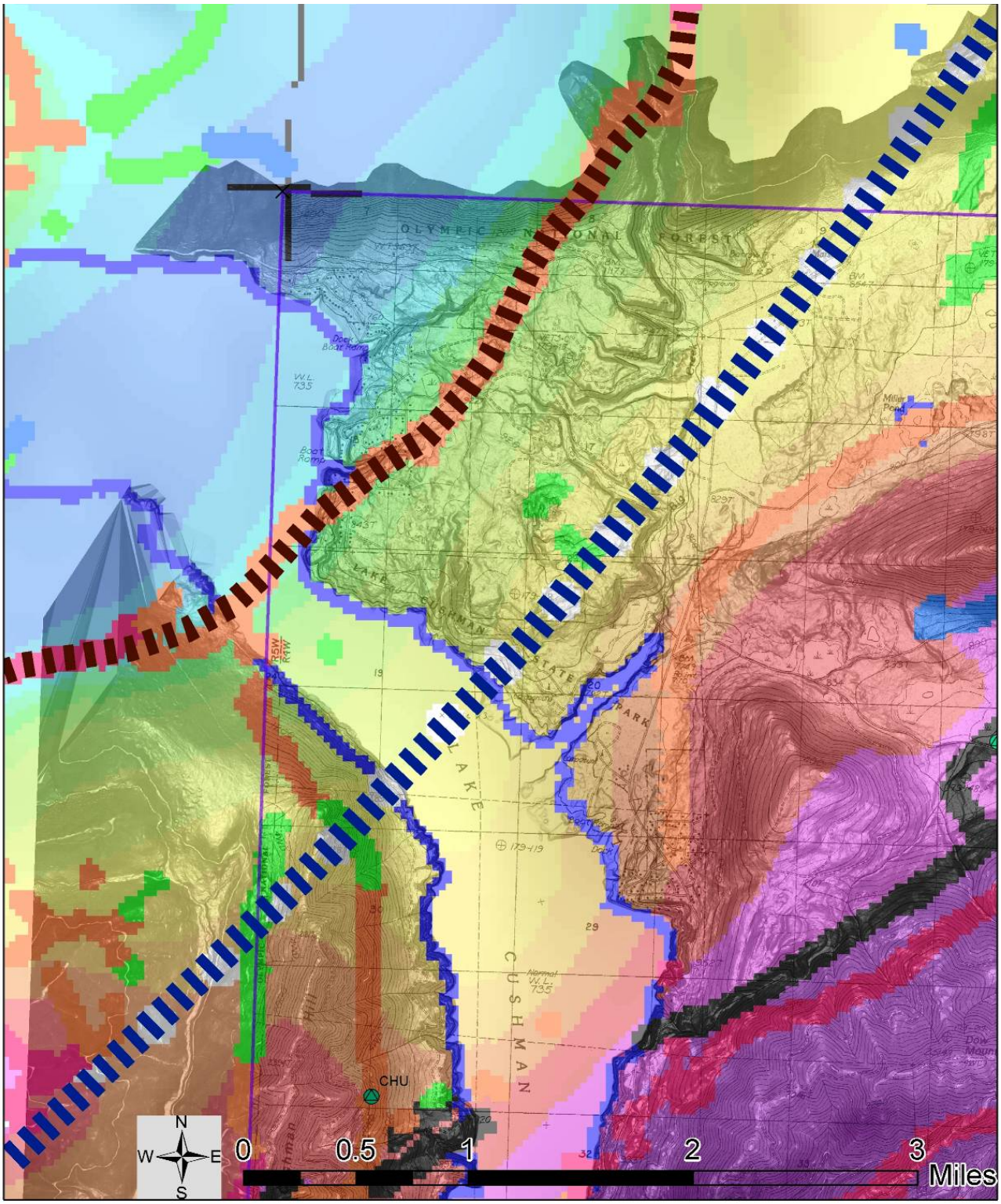

Figure 1. Geomagnetic field-strength anomalies (rainbow colors) and pole-rotated, abrupt field-strength boundaries (colored lines) near the northwest corner of Hoodsport quadrangle. (Magnetic imagery courtesy of Richard Blakely, USGS, from Blakely and others, 2009a, fig. 12A). Base map is Hoodsport 7.5-minute topographic quadrangle. Physiographic relief is a lidar hillshade image. Blue dashed line, boundary between upper and lower Crescent Formation members according to Tabor and Cady (1978). Dark brown dashed line, boundary suggested by geomagnetic gradient (orange and red backdrop beneath dashed line).

One possible advantage of this more southerly alignment of the boundary between the upper and lower members of the Crescent Formation is that it would imply a lower Crescent member association for the sample locality at CHU, which yielded an anomalously young ^{40}Ar-^{39}Ar age of 36.18 ±0.46 Ma (see Appendix A and text below; age location CHU in Polenz and others, 2012; Table 1). Given the more metamorphosed(?) character of the lower Crescent Formation member, the age estimate could then be more readily explained by thermal resetting, although the lab that provided the age estimate found no evidence to suggest that the age estimate was compromised by diffusion loss (Robert Duncan, Oregon State Univ., written commun., 2011).

Like previous mappers (Carson, 1976; Tabor and Cady, 1978; Logan, 2003), we assigned the above-mentioned ^{40}Ar-^{39}Ar sample site (age location CHU on the east slope of Cushman Hill in Polenz and others, 2012) and all other igneous exposures in the map area to the Crescent Formation. The new age estimate is anomalous, however, because previous estimates have suggested that Crescent basalt volcanism dates to between 58 and 45 Ma, with the following 10 Ma dominated instead by regional accumulation of sedimentary rocks (Babcock and others, 1994). Perhaps affiliation with another basaltic unit merits consideration.

We found igneous rock exposures in the Hoodsport quadrangle to be volcanic flows or pillows; we found relatively few dikes. Many exposures are brecciated, tachylitic, or palagonitized. Seven of eight igneous samples that we selected for whole rock geochemical analysis (geochemistry sample sites in Polenz and others, 2012) are subalkaline tholeiitic basalts that show limited major element variation (47.3–48.9 wt. % SiO_2; 6.1–7.4 wt. % MgO). The other sample is a dacite (Table 1). Thin section petrographic analysis of the dacite suggested that it is a tuff. The dacite sample site on the west shore of Lake Cushman (geochemistry sample site LCW in Polenz and others, 2012) reveals sheeted to massive and locally pillowy volcanic bedrock that is not obviously different in appearance from the generally basaltic volcanic bedrock exposures in the quadrangle. The basalt samples display slight light rare-earth enrichment (La/YbN = 0.7–3.4) and trace element affinities of mid-ocean ridge and intraplate lavas. The dacite also has intraplate affinities and, based on its high levels of incompatible trace elements (for example, U, Zr), is probably a differentiate of Crescent Formation basalt. Due to this apparent association with the Crescent Formation and the fact that its outcrop does not provide a clear basis for distinction from Crescent Formation exposures elsewhere in the map area, we chose to map the dacite as part of the Crescent Formation.

SEDIMENTARY ROCKS ABOVE THE CRESCENT FORMATION

East to southeast of Dow Mountain, marine rocks were initially mapped by Wilson (1975) and Carson (1976) as Twin River Formation. Later mappers assigned the tuffaceous marine mudstone, siltstone, and sandstone to the Eocene to Oligocene Lincoln Creek Formation (Tabor and Cady, 1978; Logan, 2003). Our mapping (Polenz and others, 2012) generally confirmed the above bedrock characterization and distribution trends, although we chose not to include the marine sedimentary rock exposures east to southeast of Dow Mountain with the Lincoln Creek Formation because we were unable to locate prior records of supporting biostratigraphic data, and several samples we collected failed to yield enough foraminifera (or diatoms) to constrain the sample ages (Elizabeth Nesbitt, Burke Museum of Natural History and Culture, written commun., 2010). However, we mapped these rocks as Oligocene–Eocene on the rationale that they are exposed upsection of Crescent Formation outcrops and their rhythmitic (turbidite?) character is inconsistent with the subaerial environment that previous research (for example, Haugerud, 2005; Mullineaux and others, 1959) suggests was established in the Puget Lowland by the Miocene.

BEDROCK TYPES FROM WHICH QUATERNARY DEPOSITS ARE DERIVED

Sediments in the Hoodsport quadrangle are derived primarily from Crescent Formation basalt and marine sedimentary rocks, Eocene to Oligocene sedimentary rocks that overlie the Crescent Formation in parts of the quadrangle, and Olympic Mountains “core rocks” and “peripheral rocks” (Tabor and Cady, 1978) exposed in the North Fork Skokomish River drainage northwest of the quadrangle. The “core rocks” of the Olympic Mountains consist of an uplifted subduction complex of disrupted and partly metamorphosed Eocene to Miocene marine sedimentary rocks (Tabor and Cady, 1978). The core rocks are mantled to the north, east, and south by a belt of “peripheral rocks” (Tabor and Cady, 1978) grouped by Hirsch and Babcock (2009) into the basalt-rich “Crescent Terrane”. In the headwaters of the North Fork Skokomish River, these rocks are in part metamorphosed to the chlorite-epidote facies (core rocks) or the prehnite-pumpellyite facies (peripheral rocks) and include sandstone (ranging from lithic to basaltic lithic, lithofeldspathic, feldspatholithic, and feldspathic, and also including some micaceous and (or) calcareous sandstone), siltstone, slate, some argillite, basalt, basalt breccia, diabase, gabbro

(partly altered to variolitic greenstone), slate, phyllite, semischist, greenstone, (vein-) quartz, and red limestone (Tabor and Cady, 1978).

Table 1. Geochemical analyses of volcanic bedrock samples from the Hoodsport quadrangle (all from this project). Sample locations are noted as geochemistry sample sites in Polenz and others (2012). Analyses by ALS Chemex, N. Vancouver, BC, Canada. Lab states that accuracy is 5% for ME-XRF06 (major element oxides, unnormalized) and 10% for ME-S81 (trace elements). LOI, loss on ignition. Rock type determined per TAS classification as presented in Walker and Cohen (2006).

Sample location		**MCS**	**LCW**	**LK**	**DMW**	**CHS**	**CHU**	**DME**	**DMR**
Unnormalized major element oxides		**Meadow Creek Spillway**	**Lake Cushman West**	**Lake Kokanee**	**Dow Mountain West**	**Cushman Hill South**	**Cushman Hill Upper**	**Dow Mountain East**	**Dow Mountain Ridge**
		Basalt	Dacite	Basalt	Basalt	Basalt	Basalt	Basalt	Basalt
SiO_2	%	46.20	63.03	45.00	46.50	46.47	45.19	46.70	47.00
TiO_2	%	1.69	0.32	1.71	2.10	1.68	2.29	2.03	2.15
Al_2O_3	%	13.60	15.00	14.46	13.73	14.57	16.10	14.40	13.75
Fe_2O_3	%	13.20	4.20	9.93	12.55	12.86	11.79	12.53	13.15
Cr_2O_3	%	0.05	0.02	0.05	0.03	0.02	0.02	0.03	0.02
MgO	%	7.03	1.22	6.63	6.25	6.58	5.81	6.93	6.51
MnO	%	0.22	0.07	0.14	0.19	0.21	0.15	0.21	0.17
CaO	%	10.10	4.35	11.24	11.64	11.62	10.53	11.41	9.58
Na_2O	%	2.98	2.90	2.46	2.30	2.33	2.94	2.18	3.52
K_2O	%	0.34	1.53	0.17	0.13	0.09	0.48	0.13	0.15
P_2O_5	%	0.16	0.04	0.14	0.20	0.14	0.21	0.19	0.20
LOI	%	4.36	7.08	8.1	3.48	3.35	4.63	3.16	3.85
Total	%	99.93	99.76	100.03	99.10	99.92	100.14	99.90	100.05

Major element oxides normalized to 100% anhydrous		**MCS**	**LCW**	**LK**	**DMW**	**CHS**	**CHU**	**DME**	**DMR**
		Basalt	Dacite	Basalt	Basalt	Basalt	Basalt	Basalt	Basalt
SiO_2	%	48.34	68.01	48.95	48.63	48.12	47.32	48.27	48.86
TiO_2	%	1.77	0.35	1.86	2.20	1.74	2.40	2.10	2.23
Al_2O_3	%	14.23	16.18	15.73	14.36	15.09	16.86	14.89	14.29
Fe_2O_3	%	13.81	4.53	10.80	13.12	13.32	12.34	12.95	13.67
Cr_2O_3	%	0.05	0.02	0.05	0.03	0.02	0.02	0.03	0.02
MgO	%	7.36	1.32	7.21	6.54	6.81	6.08	7.16	6.77
MnO	%	0.23	0.08	0.15	0.20	0.22	0.16	0.22	0.18
CaO	%	10.57	4.69	12.23	12.17	12.03	11.03	11.79	9.96
Na_2O	%	3.12	3.13	2.68	2.41	2.41	3.08	2.25	3.66
K_2O	%	0.36	1.65	0.18	0.14	0.09	0.50	0.13	0.16
P_2O_5	%	0.17	0.05	0.15	0.21	0.15	0.22	0.20	0.21
Total	%	100.00	100.00	100.00	100.00	100.00	100.00	100.00	100.00

Trace elements		MCS	LCW	LK	DMW	CHS	CHU	DME	DMR
		Basalt	Dacite	Basalt	Basalt	Basalt	Basalt	Basalt	Basalt
Ag	ppm	<1	<1	<1	<1	<1	<1	<1	<1
Ba	ppm	49.6	575	38.3	47	27.4	107.5	38	51.7
Ce	ppm	16.2	32.2	21	32.4	19.1	30.3	24.5	28.5
Co	ppm	52.5	4	43.4	48.2	53	43.1	48.1	45.2
Cr	ppm	220	200	340	170	170	170	210	200
Cs	ppm	<0.01	0.16	0.01	0.03	<0.01	0.07	0.01	0.03
Cu	ppm	188	20	110	174	182	167	170	178
Dy	ppm	6.02	12.3	4.69	5.49	5.66	4.97	4.81	5.25
Er	ppm	3.8	8.61	2.76	3.18	3.49	2.84	2.95	3.11
Eu	ppm	1.53	2.74	1.42	1.78	1.42	1.7	1.5	1.64
Ga	ppm	19.7	19.8	17.5	19.8	20.9	20.2	19.4	20
Gd	ppm	4.72	8.09	4.03	4.96	4.45	4.68	4.23	4.84
Hf	ppm	3	11.3	2.7	3.7	3	3.4	3.1	3.6
Ho	ppm	1.35	2.84	1.02	1.21	1.21	1.13	1.06	1.11
La	ppm	5.9	10.5	8.7	13.8	8.5	11.9	9.8	12
Lu	ppm	0.53	1.58	0.37	0.5	0.46	0.47	0.42	0.38
Mo	ppm	<2	<2	<2	<2	<2	<2	<2	<2
Nb	ppm	5.5	22.1	8.9	13.5	6.6	13.4	9.8	12
Nd	ppm	13.4	24.1	13.9	19.6	13.3	19.1	15.9	17.8
Ni	ppm	55	<5	77	50	51	38	52	54
Pb	ppm	8	35	5	12	<5	5	<5	<5
Pr	ppm	2.52	5.26	3.03	4.52	2.75	4.35	3.49	3.95
Rb	ppm	1.7	48.5	1.8	1.4	<0.2	5	0.4	2.3
Sm	ppm	4.29	7.93	3.84	5.19	4.05	5.08	4.45	4.62
Sn	ppm	1	3	<1	<1	<1	<1	<1	<1
Sr	ppm	252	2910	174	261	174	611	201	352
Ta	ppm	0.4	1.5	0.6	0.9	0.5	0.9	0.6	0.8
Tb	ppm	0.96	1.9	0.79	0.99	0.85	0.92	0.79	0.83
Th	ppm	0.58	4.32	0.74	1.45	0.74	1.26	0.89	1.12
Tl	ppm	<0.5	<0.5	<0.5	<0.5	<0.5	<0.5	<0.5	<0.5
Tm	ppm	0.58	1.44	0.39	0.49	0.46	0.47	0.38	0.36
U	ppm	25.5	140.5	10.5	46.8	11.65	24.3	9.29	13.65
V	ppm	342	6	321	346	388	321	335	366
W	ppm	1	1	1	4	3	4	4	4
Y	ppm	33.9	65.2	25.1	28.8	33.1	25.2	27	28.4
Yb	ppm	3.51	9.87	2.52	2.92	3.31	2.53	2.66	2.84

Trace elements *(Continued)*		MCS	LCW	LK	DMW	CHS	CHU	DME	DMR
		Basalt	Dacite	Basalt	Basalt	Basalt	Basalt	Basalt	Basalt
Zn	ppm	120	115	103	122	121	116	111	120
Zr	ppm	121	457	107	154	114	145	131	151

Quaternary Deposits

Since the end of the last glaciation, the introduction of North Fork Skokomish drainage sediment into the map area has been limited to the North Fork Skokomish valley, which for the most part is deeply incised and actively eroding in the map area and, therefore, does not result in appreciable accumulation of deposits (except beneath the natural Lake Cushman in the northwest corner of the quadrangle (see Fig. 5) and where the river has historically been dammed into Lake Kokanee and the enlarged, present-day Lake Cushman). Previous nonglacial interludes presumably have in similar fashion failed to introduce notable accumulations of Olympic-source rocks into the map area. Repeated Olympic glacial ice advances, in contrast, spread sediment derived from rock types found in the modern North Fork Skokomish drainage basin throughout the quadrangle, mostly as outwash braid-plain deposits. In addition, repeated advances of the continental Cordilleran ice sheet introduced sediment from the eastern fringe of the Olympic range, Green and Gold Mountains, the San Juan Islands, the Canadian Coast Ranges, and perhaps the northwestern Cascades. For the most part, these sediments are similar to those from the North Fork Skokomish River drainage, not least because they appear to be volumetrically dominated by contributions from the peripheral rocks of the eastern Olympic Mountains. However, they also contain plutonic and high-grade metamorphic rocks that are not found in the Olympic Mountains (Tabor and Cady, 1978; Brown and Dragovich, 2003) and are thus referred herein as diagnostically “northern”. These most prominently include granitic clasts that are readily distinguished from the above-mentioned Olympic Mountains-sourced (hereinafter “Olympic”) rocks and provide the principal tool for distinguishing northern-sourced sediment from Olympic sediment within the quadrangle. While this concept is clear and simple, in practice, diagnostically northern-source rocks are commonly diluted to much less than 1% of the clasts in outcrops of northern-source sediment in the Hoodsport quadrangle, and consequently the tool is ineffective for identification of some northern-sourced sediments (see also “Introduction” and “Description of map units” in Polenz and others, 2012). This dilution of diagnostically northern rocks, along with mixing of northern and Olympic rocks among some sedimentary deposits within the Hoodsport quadrangle, is a major source of difficulty for accurate mapping of sediments. Apparent Quaternary stratigraphic complexity is another and is discussed below.

Quaternary Stratigraphy

Unconformities, weathering, paleosols, and field relations with deposits outside the Hoodsport quadrangle suggest a broad age range for the sediments in the map area, with more stratigraphic complexity than we have been able to demonstrate or untangle. Olympic Mountains–sourced tills noted on the Kitsap Peninsula by Contreras and others (2010) indicate that Olympic ice repeatedly extended east of the modern Hood Canal, and Bretz (1913) inferred that “Vashon Epoch” Olympic ice from discrete drainage basins coalesced to form a broad piedmont ice mass there. We suspect that any Olympic ice mass that extended east of the modern Hood Canal preceded the Fraser Glaciation. We equate the Fraser Glaciation to MIS2—marine oxygen isotope stage 2[1] (Morrison, 1991; see also fig. 1 and discussion of “Late Pleistocene(?) Glacial Deposits of Undifferentiated or Pre-Vashon Age” in Polenz and others, 2012). Polenz and others (2010a,b, significant site M667, 3.75 mi southeast of the Hoodsport quadrangle) inferred depositional ages ranging from MIS2 through at least MIS5 for an apparent mix of northern-source and Olympic glacial and nonglacial deposits. Others have demonstrated mid- or early Pleistocene age for some deposits in and near the Hoodsport quadrangle (Carson, 1976; Naeser and others, 1984; Westgate and others, 1987; Easterbrook and others, 1988; Birdseye and Carson, 1989; Smith and others, 2007; Polenz and others, 2010a,b). Easterbrook and others (1988) located the type section for the Olympic Clark Creek Drift along the shore of Hood Canal within the Hoodsport quadrangle (north of the town of Hoodsport, 0.6 mi south of Clark Creek, road cuts west of U.S.

[1] Throughout this text, “MIS” (marine oxygen isotope “stage”) is used to identify glacial and nonglacial periods in the map area, as illustrated in Booth and others, 2004. Even stage numbers correspond to northern-source glacial advances, odd numbers to nonglacial intervals. Higher stage numbers identify older climatic intervals. “Stades”, such as the Vashon Stade during the Fraser Glaciation, identify shorter intervals within stages.

Highway 101; stratigraphic column site CCTS in Polenz and others, 2012), and they defined the unit as correlative to the magnetically reversed, early Pleistocene Salmon Springs Drift. Similarly, Easterbrook and others (1988) introduced the northern-sourced Annas Bay Drift with a type section 1 mi south of the map area (see also stratigraphic column location ABTS in Polenz and others, 2010a) as correlative to the Salmon Springs Drift, and Molenaar and Noble (1970) introduced the Olympic Skokomish Gravel with its type section 4 mi south of the map area (see also stratigraphic column location SGTS in Polenz and others, 2010a) as correlative to MIS3, although a reinterpretation by Carson (1979), stratigraphic arguments by Carson (1980), and an age estimate by Polenz and others (2010a,b, age-date sample locality M470) suggest a much greater age for at least part of that section.

Polenz and others (2010a,b) suggested that the valley walls along the main stem Skokomish River (4 mi south of the Hoodsport quadrangle) contain a complex patchwork of glacial and nonglacial deposits of diverse and mostly undocumented Pleistocene ages. They found that stratigraphic diversity was less clearly apparent but may be equally prevalent along the valley walls of the North Fork Skokomish River, where deposits are dominated by thick, gravel-rich packages of glacial drift of mostly Olympic-source lithology. We saw a similar pattern along the valley walls of Frigid Creek, McTaggert Creek, Finch Creek, and the North Fork Skokomish River, the main differences being that glaciolacustrine deposits are more common in the Hoodsport quadrangle than south of it, and along the North Fork Skokomish River, bedrock commonly extends to less than 100 ft below the upland surface. In light of the stratigraphic complexity and limited age-constraining data for Pleistocene deposits in the area, we continue with the approach of Polenz and others (2010a,b, 2012), who incorporated the more restrictive Pleistocene units employed by some workers into less restrictive map units because more work will be needed to develop a truly satisfactory model of the Quaternary stratigraphy in the map area.

While improved age control will be central to any successful attempts to further resolve the stratigraphy of sediments in the Hoodsport quadrangle, numerous age-control data points have been generated within and near the quadrangle. Most of these resulted from fault trench investigations and pertain to Holocene deposits. For Pleistocene deposits, the radiocarbon, tephrostratigraphic, optically stimulated luminescence, and paleomagnetic data summarized by Polenz and others (2010a,b) in their discussions of the Skokomish Valley and Union quadrangles may be as insightful as those available within the Hoodsport quadrangle. The data discussed by Polenz and others (2010a,b) include a tephra from the southern valley wall of Frigid Creek in the southwest corner of the Hoodsport quadrangle, and while the fission track age estimate from that tephra is presented again below, we refer to Polenz and others (2010b) for discussion of chemical attributes of the tephra and attempts to relate this tephra to tephra exposures elsewhere.

Age-Control Data

Age-control data from within the Hoodsport quadrangle (and data from one fault trench investigation 1,500 ft west of the quadrangle) are compiled in Appendix A. A large number of fault investigations in this area have spawned a wealth of age-control data. We compiled age-control data from this study (five dates), all fault trench investigations, other studies within the quadrangle, and a trench investigation of the Frigid Creek fault 1,500 ft west of the quadrangle. The Frigid Creek fault trench investigation was included here because it characterizes a fault that clearly extends into the quadrangle. Of 49 direct age estimates, 42 pertain to fault investigations, and of those 42, 22 have been previously published, although many of those lacked the level of documentation provided by the compilation in Appendix A. The other 20 fault investigation dates were obtained by Jonathan Hughes while he worked at the USGS. (He now works at the University of the Fraser Valley and is a coauthor of this report.) Hughes' dates have until now not been presented as individual data points. Instead, Hughes (2005) used these dates and analysis of sediment cores and samples of wood from coseismically submerged stumps (Fig. 2) to develop constraints on dip-slip magnitude and timing of Holocene fault rupture on the Saddle Mountain East and West strands at Price Lake. Our compilation now includes Hughes' individual age-control data points. In addition, Hughes obtained a geochemical analysis of a tephra sample from a wetland located tens of meters south of Price Lake (Fig. 3; geochemical sample site ASH in Polenz and others 2012). Assuming that the tephra is correctly associated with the climactic Mount Mazama eruption (Fig. 3), which has been dated to 7.6 ka (Zdanowicz and others, 1999; Hallett and others, 1997), this tephra constrains the post-glacial rate of sedimentation in the wetland south of Price Lake.

Figure 2. Douglas-fir (*Pseudotsuga menziesii*) stump top at the western edge of Price Lake, Washington. This sample supplied the radiocarbon ages provided as H5a and b in Appendix A. Brian Atwater (pictured) is using a chainsaw without chain oil, to minimize environmental impacts. Additional stumps in back are similarly submerged.

Timing and Duration of Vashon Ice in the Hoodsport Quadrangle

Two new ^{14}C age estimates from glaciolacustrine deposits below Vashon till (age-date sample sites SCVA and UFCVA in Polenz and others [2012]; Appendix A) constrain the timing of Vashon (Puget lobe) ice arrival in the map area to approximately between 17,000 and 15,700 cal yr B.P. (calendar years before 1950). Sample UFCVA (Figs. 4a,b) was collected at about 550 ft elevation, and sample SCVA at about 1,070 ft, south and east, respectively, of Dow Mountain. These elevations are too high to be part of the large lake that would have been impounded south of the advancing Puget lobe ice and drained south to the Chehalis River. They therefore require that when our samples were deposited, Puget lobe ice was close enough to dam smaller, more elevated lakes against the local slopes. The presence of the lakes and fragile organic debris amid the lakes' muddy sediment suggests that the map area was not yet fully overwhelmed by the approaching Puget lobe ice mass. Consequently, deposits at age-date sample site UFCVA (see Figs. 4a,b below) and a similar, more elevated site 2.4 mi north-northeast (age-date sample site SCVA, Polenz and others, 2012, and Appendix A) closely constrain the time of Vashon Puget lobe ice arrival. The age estimates from both sample sites date detrital organic matter that could have introduced in-built age, such that depositional ages could be slightly younger (Gavin, 2001). In-built ages in both samples are probably insignificant, however, because the organic matter consisted of small wood fragments that would not likely have persisted long prior to burial. At SCVA, the sample consisted of twig fragments; sample site UFCVA included soft organic debris (see Fig. 4b).

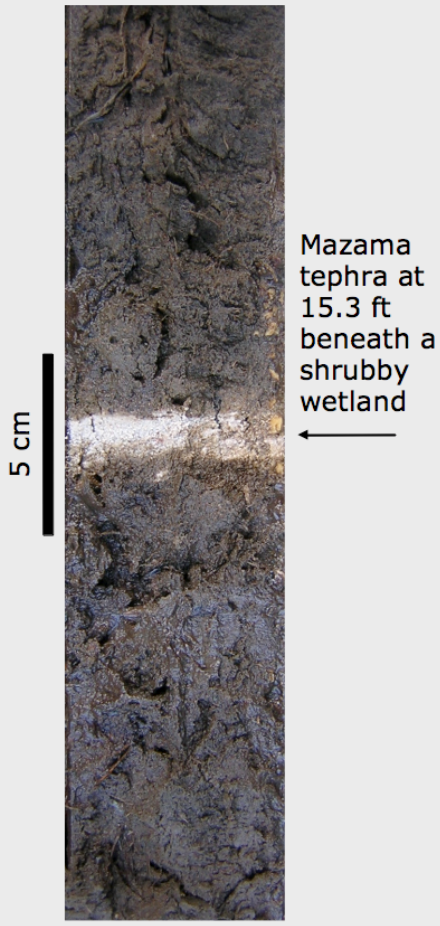

Glass chemistry of Puget Sound Mazama climactic tephra compared with a tephra collected from a wetland located on the southern edge of Price Lake, Washington.

Oxide	PL-467[a]	Mazama climactic tephra[b]
SiO_2	73.31(0.20)	73.29(0.24)
Al_2O_3	14.49(0.14)	14.43(0.11)
Fe_2O_3	2.10(0.05)	2.12(0.06)
TiO_2	0.42(0.03)	0.43(0.02)
Na_2O	4.70(0.21)	4.79(0.19)
K_2O	2.75(0.04)	2.69(0.05)
MgO	0.46(0.03)	0.47(0.03)
CaO	1.62(0.05)	1.61(0.05)
Cl	0.15(0.02)	0.16(0.02)
Totals[c]	100	100
Analytical totals	96.92(2.87)	96.94(2.38)
Shards analyzed	15	17
Similarity coefficient[d]	0.99	

[a] Standard deviations of the analyses given in parentheses.
[b] Foit and others (2004)
[c] Analyses normalized to 100 weight percent on a volatile-free basis.
[d] Borchardt and others (1972) search weighting: Si, Al, Fe, K, Ca, Na = 1.0; Mg and Ti = 0.25.

Figure 3. Tephra found beneath a wetland on the southern edge of Price Lake, geochemistry sample site ASH in Polenz and others (2012). Franklin Foit, Washington State Univ., identified the volcanic ash as originating from the Mount Mazama climactic eruption ~ 7627 ±150 cal yr B.P. (Zdanowicz and others, 1999). Sample was collected on July 21, 2005, by Jonathan Hughes (Univ. of the Fraser Valley) and Robert Carson, Christopher Iacoboni, and Morgan Zeliff (all three Whitman College).

The determination of the timing of Vashon Stade arrival of Puget lobe ice in the Hoodsport quadrangle permits an improved assessment of the stratigraphic context and significance for a previously documented ^{14}C age estimate from 7 mi south of the Hoodsport quadrangle, where Polenz and others (2010a) estimated that a western hemlock (*Tsuga heterophylla*) tree from apparently lacustrine mud beneath a gravel quarry died between 15.7 and 15.3 ka (see age date site M831 of Polenz and others, 2010a). The log had emerged with "blue clay" mud when a quarry dredge scooped this muddy sediment from beneath the base of a recessional gravel outwash deposit. The gravel outwash is part of a broad recessional outwash deposit that partly fills a complex of meandering outwash channels incised into the surrounding fluted uplands (and associated Vashon till deposits) between Oakland Bay (northeast of Shelton) and the Skokomish Valley (Polenz and others, 2010a,b). The pit operator characterized the "blue clay" as a homogeneous mud deposit at least 4 ft thick and extending across more than 2.5 acres, suggestive of a (glacio?) lacustrine deposit. Because the outwash channel is eroded into the surrounding upland surface and the substrate was not exposed, it was unclear to Polenz and others (2010b,a) whether the blue mud and the log it contained were deposited prior to or following the presence of Vashon ice in the area, although post-ice deposition seems unlikely because it would require glaciorecessional incision of an outwash channel into the surrounding upland surface followed by emergence of a lake that would support deposition of a homogeneous and relatively extensive mud layer, followed in turn by renewed glaciorecessional drainage that deposited a large volume of additional recessional gravel within the outwash channel complex. Deposition of the blue mud prior to the arrival of Vashon ice, in contrast, is readily explained by

Figure 4a. Vashon advance glaciolacustrine sediment (primarily laminated mud) at age location UFCVA of Polenz and others (2012). Although the glaciolacustrine deposits are predominantly horizontally laminated, beds locally bend up to cover sloping surfaces (such as in lower half of image), and some beds dip in excess of 30 degrees. These relatively steep dips are interpreted herein as mostly depositional because the dipping beds and their more level, lateral continuations generally lack the distortion and discontinuities typically associated with ice shove or other mechanisms of post-depositional deformation. Cobbly material in the lower right is interpreted as a gravity flow deposit. The glaciolacustrine character of this cobbly deposit is supported in part by a pervasive muddy matrix and by its conformable integration into what is overall a section dominated by muddy to sandy lacustrine beds and laminae. Similar gravelly glaciolacustrine deposits are common in unit Qga, especially around Dow Mountain, and in older glaciolacustrine deposits elsewhere in the Hoodsport quadrangle. The gravity flow deposits were fed from either local slopes or the approaching Vashon Puget lobe ice mass (both sources are widespread in unit Qga). The presence of gravity flow deposits from Puget lobe ice suggests that the Cordilleran ice sheet had arrived in the map area at the time of lake sediment deposition at this site. The 550 ft site elevation at UFCVA requires that the lake was localized and dammed by ice against the eastern flank of Dow Mountain. Blue coating on tool handle is 16 in. (41 cm) long; handle diameter is 1⅜ in. (3.7 cm).

the development of a large proglacial lake that would fill the southern Puget Lowland once Cordilleran ice dammed the Strait of Juan de Fuca. Moreover, the incision of the outwash channel complex into the surrounding upland suggests that the Vashon till has been removed from the site. These considerations, while not conclusive, favor a pre-Vashon age for the log dated by Polenz and others (2010a). The estimated time of tree death at 15.7 to 15.3 ka coincides relatively closely with the 17 to 15.7 ka time of Vashon ice arrival now determined for the Hoodsport quadrangle. This age interpretation strengthens the argument that the quarry log records the time of the approaching Vashon ice and improves confidence that the time of Vashon ice arrival is well constrained by all three ^{14}C age estimates. The somewhat younger age estimate of the quarry log is perhaps attributable to its location 10 mi south of sample site UFCVA.

No previous study has focused on the timing of Vashon ice arrival near the map area, but Porter and Swanson (1998; for an improved illustration, see fig. 9 in Booth and others, 2004) used data from the central and eastern Puget Lowland to estimate the timing of both the advance and retreat of the Vashon ice in the region. Their

Figure 4b. Conifer needles in laminated to massive glaciolacustrine mud at age location UFCVA (Polenz and others, 2012). (Pencil in lower right is 0.33 in. [0.85 cm] wide, its tapered tip 0.75 in. [1.9 cm] long.) Conifer needles such as those in the center of the image are part of ^{14}C age-date sample UFCVA (Appendix A) and together with age date sample FCVA (Appendix A) have helped constrain the arrival of Vashon Puget lobe ice at Dow Mountain to between 17 and 15.7 ka (see text above and below for additional discussion and regional significance).

estimates would suggest that the Puget Lowland was largely post-glacially ice free by about 16,000 cal yr B.P (~16 ka). In contrast, our new age estimates indicate that the Hoodsport quadrangle and areas to its south remained pre-glacially ice free until about that time. This paradox resembles previously noted age constraints for the Vashon ice arrival in the southeastern Puget Lowland, where Walsh and others (2003) documented that Vashon ice had not yet arrived on the upper slopes of the eastern valley wall of the lower Nisqually Valley by 13,410 ±80 ^{14}C yr B.P., equivalent of about 16.6 to 15.7 ka (16,580–15,740 cal yr B.P.)[2]. Similarly, a 13,630 ±90 ^{14}C yr B.P. age estimate (Beta-52222, 16,450–15,980 cal yr B.P.)[3] on pre-Vashon peaty sediment from a borehole 0.5 mi north of Sequalitchew Lake, Fort Lewis 7.5-minute quadrangle[4], suggests a Vashon ice arrival later than the timeline of Porter and Swanson. These indications of a "late" Vashon ice arrival in the southern Puget Lowland coupled with Porter and Swanson's (1998) indications for nearly coeval, post-glacially ice-free conditions elsewhere in the Puget Lowland are consistent with speculations (Haugerud, 2009; Logan and Walsh, 2009) that much or all of the Vashon Puget ice sheet stalled and quickly began to disintegrate once it had reached its southern terminus, although Porter

[2] 2-sigma calibrated age range per Beta Analytic report, unpub. records of Michael Polenz.
[3] 2-sigma calibrated age range per Beta Analytic written commun. to Michael Polenz, 2011.
[4] Unpublished records of Tim Walsh, Wash. Division of Geology and Earth Resources; sample courtesy Alan Carey of AGI, from 60 ft below surface, MW-12B, sec. 19, T19N R2W; borehole stratigraphy approximates that described by Noble (1990), p. 46, for a nearby well; dated material was peaty silt from "Discovery nonglacial unit" described by Noble between 162 and 154 ft elevation.

and Carson (1971) demonstrated that patches of residual, stagnant ice may well have persisted for centuries or millennia.

Fraser(?) Olympic Ice in the Map Area

Previous workers Bretz (1913), Long (1975, 1976), and Carson (1980) have advocated the notion that Vashon (Puget lobe) and coeval MIS 2 Olympic alpine ice collided at the northwest corner of the Hoodsport quadrangle. Long (1976) further suggested that Olympic ice "readvanced after the maximum of the most recent Puget Lobe and overlapped Vashon drift at mid-Lake Cushman." Although we did not discover evidence for or against a meeting of Vashon Puget lobe and Olympic ice, we noted that lidar-based hillshade images with selected illumination angle(s) reveal a valley-parallel fabric in the surface morphology of the west half of unit Qgim east of (the natural portion of) Lake Cushman (Polenz and others, 2012; Fig. 5). This fabric may be best interpreted as fluting from east-southeast-directed ice flow of an Olympic-sourced glacier in the North Fork Skokomish valley, consistent with the Olympic-ice readvance advocated by Long (1976).

While the apparent fluting (Fig. 5) provides evidence for an Olympic alpine ice advance that post-dated the presence (or dominance) of Vashon Puget lobe ice in the area, the Olympic ice seems to have only surficially scratched the underlying, lumpy landform, and we found no evidence that this MIS 2 (or later?) Olympic ice produced lodgment till deposits of mappable thickness and extent, although we caution that we saw few exposures in this area. The exposures we saw typically revealed thick sections of sand or gravel that are readily interpreted as part of a terminal moraine (but lack a capping sheet of lodgment till). We and previous workers (Bretz, 1913; Long, 1975,) broadly interpret the area as the Vashon Puget lobe ice limit, and we interpret the sandy and gravelly exposures within it as Vashon Puget lobe moraine (unit Qgim), both where overprinted by apparent fluting from Olympic ice (west of alpine ice limit in Fig. 5), and farther east, where we did not recognize fluting.

Shores of Ice-dammed Lake(s?) along Hood Canal

Map units Qgol and Qgl_s (Polenz and others, 2012) are tied to the former presence of an ice-dammed lake (or lakes?) in southern Hood Canal. We identified lakeshore delta deposits (unit Qgol) above the west shore of Hood Canal in three locations within the Hoodsport 7.5-minute quadrangle, as well beach deposits (unit Qgl_s) and associated strandlines. Contours on the U.S. Geological Survey 7.5-minute topographic map of the Hoodsport quadrangle indicate topset-foreset slope break elevations between 210 and 240 ft, but more precise (and likely more accurate) lidar data indicate levels between about 230 and 250 ft (see Table 2). Similar shorelines were noted by Polenz and others (2010a,b) in the Skokomish Valley quadrangle south of the Hoodsport map area, and Polenz and others (2010b) contemplated a lake surface elevation at about 220 to 240 ft as a possible southern Hood Canal lake level south and east of the Hoodsport quadrangle. Polenz and others (2010b) suggested that this lake, like Lake Skokomish as previously contemplated by Bretz (1913) and Thorson (1981), and Lake Hood as envisioned by Bretz (1913), would have drained south to Lake Russell. The observation as part of the Hoodsport quadrangle mapping project of shoreline deposits (units Qgl_s and Qgol) between about 230 and 250 ft provides additional evidence that, at least for some time, a sizeable proglacial lake (or lakes) existed in the area.

Figure 5. *(facing page)* East-southeast-trending fabric in the surface morphology of the western half of a lumpy hill east of Lake Cushman in the northwest corner of the Hoodsport quadrangle. (Figure is oriented north-up.) The fabric is distinct west of the blue-green, convex-east arc across the image and appears to be absent to the east. The hill was mapped as Vashon Puget lobe moraine (unit Qgim) by Polenz and others (2012). The east-southeast fabric does little to modify the overall morphology of the hill, and it falls short of eliminating the lumps in its surface, but it does seem to partially smooth out the surface. The fabric may be best explained as fluting from an east-southeast-moving alpine ice mass that post-dated the presence (or at least the dominance) of Vashon Puget lobe ice. The apparently fluted area is topographically lower than the eastern portion of the hill, consistent with the interpretation that glacial overriding not only scoured and fluted, but also compacted the area. The blue-green arc approximates the apparent maximum extent of the Olympic (alpine) ice advance.

The "Natural Lake Cushman" label on the right margin of the image refers to the historical record (Bretz, 1913) of a natural lake upvalley of (and impounded by) the moraine across the valley (the only part of the North Fork Skokomish valley in the Hoodsport quadrangle that was subject to sustained post-glacial sedimentary deposition prior to the construction of the dams that now impound Lakes Cushman and Kokanee). The existence of the lake suggests that an (Olympic-source) valley glacier either was present while Puget Lobe ice occupied the area to the east and south, thereby preventing infilling of the valley (to the west) by the combined sedimentation from Puget lobe meltwater and North Fork Skokomish River drainage, or that a later valley glacier scoured out the valley upvalley of the moraine, consistent with the proposition that the western portion of the moraine was overridden by Olympic ice. Map unit labels are defined in Polenz and others (2012).

Natural Lake Cushman
Qaf
Qgim
Qgic?
Qls
Qa
Qoaf
Qp
Qgic
Qgo
Qgt
Qm w
Ev(c)
PVAF
FUT
Qgoaf
Qgt?
Qa d?
Qad?
Qgo?
Qgic?
Qoa?
wtr
1300
1500
1400
1200
1100
1000
900
800
700
600
500
400
300
200
100

Table 2 provides glaciolacustrine shoreline elevation estimates from both the Hoodsport and the Skokomish Valley quadrangles. A single elevation estimate is given for each site, but it bears noting that these are approximations. Sources of uncertainty include that (1) the shorelines are for the most part only subtly expressed in the lidar data, (2) our elevation estimates may in places have been elevated by later deposition of a colluvial apron, whereas, especially on steeper slope segments, the entire feature may have crept slightly downslope, (3) individual locations may have been subjected to different fetch, and consequently different wave heights, leading to different beach top elevations, and (4) delta sites seem to display up to about 10 ft of variability in the lidar data, perhaps in part due to differential settling. The resulting set of elevation estimates clearly displays some scatter. In the Skokomish Valley quadrangle, the site "South of Potlatch State Park" is slightly north of where Polenz and others (2010a) showed a short shoreline segment, reexamination of which suggested that it may have been altered by development of topographic irregularities associated with surrounding stagnant ice deposits. A more consistent bench was identified as an apparent shoreline to the north (and likely also extends to the south), but it was classified as questionable due to disturbance by erosion and manmade land surface alterations that render this likely shoreline segment impossible to identify with certainty.

Table 2. Glacial lake delta elevation estimates in the Hoodsport and Skokomish Valley quadrangles. N/A, not applicable.

Quadrangle	Site characterization	Elevation (ft)	Distance (mi) from Purdy Canyon outwash terrace	Elevation change to Purdy Canyon	Slope (ft/mi) to Purdy Canyon
Skokomish Valley	Purdy Canyon, lowest outwash terrace (sec. 22, T21N, R4W)	240	0	0	N/A
Skokomish Valley	South of Potlatch State Park (questionable beach) (secs. 26 and 35, T22N, R4W)	220	4.6	-20	-4.348
Skokomish Valley	South of Potlatch Hydropower standpipe (beach) (secs. 26 and 27, T22N, R4W)	225	5.1	-15	-2.941
Skokomish Valley	North of Potlatch Hydropower standpipe (beach) (secs. 26 and 23, T22N, R4W)	232	5.4	-8	-1.481
Hoodsport	Northern Potlatch south (delta and beach) (sec. 23, T22N, R4W)	250	6.1	10	1.639
Hoodsport	Northern Potlatch north 1 (beach) (sec. 23, T22N, R4W)	250	6.5	10	1.538
Hoodsport	Northern Potlatch north 2 (beach) (sec. 14, T22N, R4W)	250	7	10	1.429
Hoodsport	South of Finch Creek (delta) (sec. 11, T22N, R4W)	241	7.6	1	0.132
Hoodsport	South of Miller Creek (delta) (sec. 1, T22N, R4W)	248	9.4	8	0.851
Slope yielded by 0.06° regional rebound tilt estimate of Thorson (1989).		295.3	10	55.3	5.530
Local rebound (?) tilt suggested by locally observed elevations of lake deltas and strandlines relative to each other = 0.06°.					5.53

The considerable scatter in the glaciolacustrine shoreline elevation estimates presented in Table 2 suggests the possibility that not all shoreline segments belonged to the same lake. We cannot dismiss that possibility, but we only identified a single apparent shoreline at any given latitude, suggesting that only one lake level was persistent enough and endowed with enough fetch to permit waves to cut a shoreline and assemble a beach. This does favor a single, large lake, although the scatter of the data does not.

In Figure 6, the distance north of Purdy Canyon for each shoreline elevation estimate is plotted against the elevation of the data point. On the assumption that all shoreline segments indeed were part of the same lake, a (blue) best-fit line through these shore elevation estimates yields a rebound tilt orientation that exceeds the slope from any one of these points to the putative lake drain at Purdy Canyon. However, the slope of the best fit line matches Thorson's (1989) regional tilt estimate (red line). This similarity may be coincidental, considering the scatter in the local dataset. Moreover, the intercept of the line with the putative lake outlet at Purdy Canyon is 40 ft below the

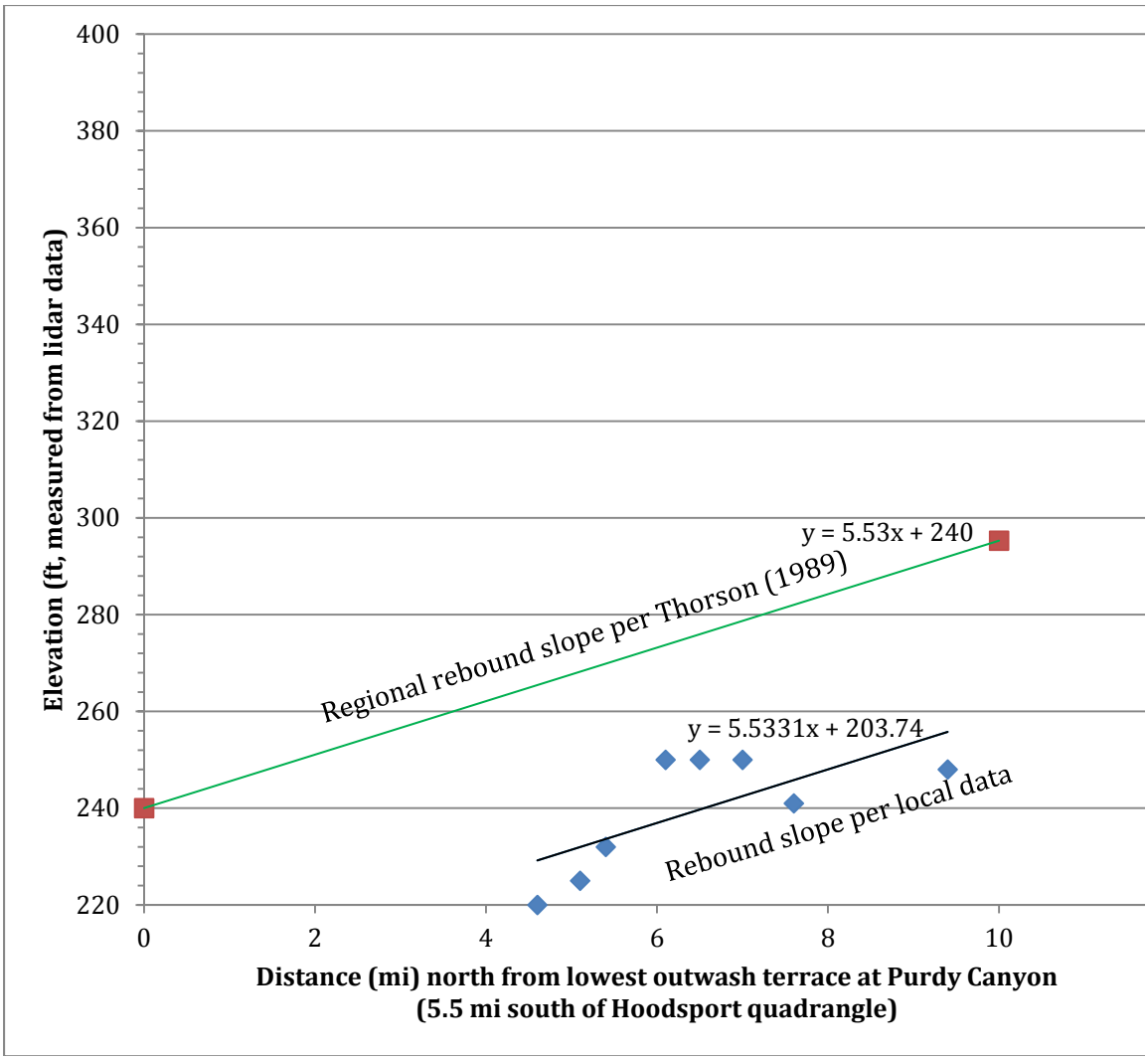

Figure 6. Regional glacio-isostatic rebound tilt slope and glaciolacustrine shoreline markers along southern Hood Canal.

lowest Purdy Canyon outwash terrace. Multiple scenarios could explain this: (1) the lake might have been drained somewhere else at a lower elevation; (2) tectonic or glacio-isostatic offset between the shoreline data points and the putative lake drain at Purdy Canyon could have elevated Purdy Canyon relative to the documented shoreline segments; and (3) the similarity of the best-fit line to the regional rebound tilt estimate of Thorson (1989) could be coincidental, with actual tilt at any one site being potentially varying from other locations (even nearby) and regional tilt more likely being the sum of a number of tectonic offsets. This last scenario may be the most likely in light of the scatter of the datapoints and the empirical evidence that rebound, as historically observed, for example, in parts of Greenland and Fennoscandia, is associated with seismic events that may locally tilt the crust but in doing so would also offset one block against an adjacent block, likely resulting in some tilt differentials as well as scatter in rebound magnitude from one site to the next. Considerable scatter in elevations of outwash surfaces noted by Haugerud (2009) on the Kitsap Peninsula east of Hood Canal may point to similar conclusions.

STRUCTURE

Tectonic Setting

The Hoodsport quadrangle is located in the forearc of the Cascadia subduction zone. Oblique convergence of the Juan de Fuca plate with North America and shear motion of the Pacific plate with respect to North America result in

margin-parallel shortening within the forearc in western Washington (Wells and others, 1998). This shortening is at least partly accommodated by a system of west- to northwest-trending, active faults across the Puget Lowland (Wells and others, 1998). McCaffrey and others (2007) estimate the rate of shortening that is accommodated by (the sum of) these faults at 4.4 ±0.3 mm/yr. The faults divide the Puget Lowland into areas of uplift and subsiding basins, identifiable in gravity and magnetic data (Daneš and others, 1965; Brocher and others, 2001; Johnson and others, 2004). The Hoodsport quadrangle may include the western boundary of crustal shortening of the Puget Lowland (Blakely and others, 2009a).

A number of potentially active structures have been identified within or potentially within the Hoodsport quadrangle. East of the Hoodsport quadrangle lies the east–west-trending Seattle uplift, bounded on the north by the Seattle fault and on the south by the Tacoma fault. Bedrock is exposed at Green and Gold Mountains between the two faults; no bedrock is exposed in the Seattle and Tacoma basins north and south of the Seattle uplift. It is unclear whether the Seattle fault and the north-directed, reverse offset associated with it cross Hood Canal along the easterly trend that prevails farther east along the Seattle fault, as suggested by Blakely and others' (2009a) and Lamb and others' (2009) interpretations of geophysical data, or if its trace turns towards the southwest east of the canal, as suggested by Lamb and others' more recent interpretation of geophysical data (A. Lamb, Boise State Univ., written commun., 2011). Similarly, it is not clear if the Tacoma fault crosses Hood Canal. Prior studies have documented the Tacoma fault as extending across the southern Kitsap Peninsula to the south shore of Hood Canal east of the Hoodsport quadrangle (Sherrod and others, 2003, 2004; Logan and Walsh, 2007; Nelson and others, 2009; Derkey and others, 2009a,b), and Contreras and others (2010) cite the Dewatto basin (Johnson and others, 2004; Blakely and others, 2009a; Lamb and others, 2009) and deformed glaciolacustrine sediments as evidence that strands of the Tacoma fault may also be present on the Tahuya peninsula—closer to the Hoodsport quadrangle, albeit still east of Hood Canal. No strand of the Tacoma fault has to date been identified west of Hood Canal, and tomographic modeling of Brocher and others (2001) and analysis of geophysical data by Lamb and others (written commun., 2011) suggest that the Tacoma fault may bend north across the Tahuya peninsula rather than extending west across Hood Canal, as had been suggested by Lamb and others' earlier (2009) interpretation. The last major earthquakes on the Seattle and Tacoma faults occurred between 900 and 930 A.D. (Atwater, 1999) and 770 and 1160 A.D. (Sherrod and others, 2003), respectively.

The northeast-trending Hood Canal fault has been inferred in the middle of Hood Canal from high resolution seismic data (Haug, 1998; Sherrod and others, 2004) and tomographic modeling (Brocher and others, 2001). It would enter the Hoodsport quadrangle in the southeast corner. Doubt has been cast on the existence of this structure by interpretations of magnetic data, which fail to reveal an associated anomaly (Lamb and others, 2009). Our mapping produced no insights regarding the existence or character of the Hood Canal fault.

The northwest-trending Olympia structure southeast of the Hoodsport quadrangle was postulated but not yet named by Daneš and others (1965). The geophysical anomalies defining the Olympia structure could be an expression of faulting or folding of Eocene bedrock, but its exact nature remains unconstrained (Magsino and others, 2003). Magsino and others noted that evidence for an earthquake in the vicinity of the structure around 900 A.D. (Sherrod, 2001) could suggest that the Olympia structure is a post-glacially active fault. The northwest-trending Lucky Dog structure, which has been documented in the Skokomish Valley south of the Hoodsport quadrangle (Polenz and others, 2010a,b), could be an expression of the Olympia structure, but if so, this is not clearly borne out by the geophysical data, which suggest that the Olympia fault is farther southeast. Below, we summarize limited geologic and geophysical data relating to whether the Lucky Dog structure may extend northwest into the Hoodsport quadrangle.

The northeast-trending Saddle Mountain fault zone (Blakely and others, 2009a), or Lidke's (2003b) "Saddle Mountain Faults", traverses the north and center of the Hoodsport quadrangle and may be the most significant structure within the map area. Post-glacially active constituent faults in this zone of deformation include the Saddle Mountain West fault, the Saddle Mountain East fault (including the Cushman Rift/Cushman Valley fault), the Frigid Creek fault, the Canyon River fault, the Dow Mountain fault, and an unnamed fault east of the Saddle Mountain East fault. Miscellaneous scarps and lineaments (Polenz and others, 2012) along the Saddle Mountain fault zone may be expressions of additional fault strands that have not yet been confirmed by trench investigation or other compelling observations. Blakely and others (2009a) present aeromagnetic data suggesting that the Saddle Mountain fault zone extents for more than 45 km along the southeast margin of the Olympic Mountains. They interpret the fault zone as the western boundary of crustal shortening of the Puget Lowland, accommodated by oblique-slip on the constituent faults. Multiple studies have documented post-glacial ground rupture and coseismic land level changes on the Saddle Mountain East and West faults (Carson, 1973; Wilson, 1975; Wilson and others, 1979;

Hughes, 2005; Witter and Givler, 2005; Witter and others, 2008; Blakely and others, 2009a; Czajkowski and others, 2009a,b; Barnett and others, 2009a,b). At least some of these occurrences have been interpreted as associated with M >6.8 earthquakes between 700 and 1,000 A.D. (Witter and Givler, 2005; Witter and others, 2008; Blakely and others, 2009a). A paleoseismic trench across the Frigid Creek fault also revealed late-Holocene offset (Blakely and others, 2009a). Additional information on these structures is discussed below.

Evidence for Post-Glacial Tectonic Effects

MAPPED FAULTS AND FOLDS

The fault strands shown in Polenz and others (2012) were modified from the Washington State Geologic Information Portal (hereinafter, the "Portal", http://www.dnr.wa.gov/ResearchScience/Topics/GeosciencesData/Pages/geology_portal.aspx, v. 2), which in turn were based largely on fault strands shown by Blakely and others (2009a). Following initial reproduction of the fault strands imported from the Portal into our project GIS files, individual strands were modified (if needed) once each strand was considered in close view (1:24,000 or larger scale) and in the context of our field observations, lidar, aerial photo imagery, geophysical data, and prior publications (Carson, 1973; Wilson, 1975; Wilson and others, 1979; Hughes, 2005; Witter and Givler, 2005; Witter and others, 2008; Blakely and others, 2009a; Czajkowski and others, 2009a,b; Barnett and others, 2009a,b). Some strands that we felt to be appropriate interpretations, even if our own mapping produced no site-specific corroborating data, were included in Polenz and others (2012) without modification from those shown in the Portal, in deference to the prior studies that had mapped them (as cited in the Portal at time of our file import). Elsewhere, we added previously undocumented strands, such as the north-trending, west-up scarps (Fig. 7) east of the Dow Mountain fault (and significant site DMFT) in Polenz and others (2012). The results of our revisions later became the basis for revisions to the fault strands shown in the Washington State Geologic Information Portal.

Aside from fault strands, we also show (in Polenz and others, 2012) clusters of scarps and lineaments aligned with and (or) near mapped fault strands. These morphologically evident but unexplained features were opportunistically identified where they caught our attention, but they do not represent the result of a systematic review of all available data. We believe that they merit consideration, but most are subtle, and none have been shown to be tectonic. One lineament 2,800 ft northeast of the southeast end of the Dow Mountain fault scarp (Fig. 8 and Polenz and others, 2012) was previously identified by Witter and others (2008, fig. 2) and Blakely and others (2009a) and was also apparent to us in lidar data. However, we show it mainly to note that field verification of the feature revealed a coincident forest road.

SADDLE MOUNTAIN FAULT ZONE

Although loggers had "encountered" scarps around Price Lake prior to 1939 (Witter and others, 2008), Carson (1973) first demonstrated the presence of a post-glacially active, northeast-trending "Saddle Mountain fault", citing a fault investigation trench and northeast-trending scarps and lineaments between Price Lake and Lilliwaup Swamp. The trench demonstrated postglacial reverse (and possible strike-slip) offset of basalt bedrock and overlying Vashon till on a southeast-dipping fault plane. Wilson (1975) introduced a parallel "Saddle Mountain West fault" strand 0.5 mi farther west and therefore renamed Carson's Saddle Mountain fault "Saddle Mountain East fault". Witter and others (2008) suggested that the Saddle Mountain East fault extends southwest to Lake Cushman, where it incorporates the "Cushman Valley fault" (Wilson and others, 1979; originally named "Cushman Rift" by Carson and Wilson, 1974).

North of the Hoodsport quadrangle, Wilson and others (1979) suggested that a north-trending zone of fractured basalt, which Glassley (1974) had presented as an apparent zone of separation between the upper and lower members of the Crescent Formation, may also be a northern extension of the Saddle Mountain faults. Richard Blakely (written commun., 2011) reinforces this possible association between the upper member–lower member contact and the Saddle Mountain faults by noting that a pronounced magnetic boundary crosses Lake Cushman where the Saddle Mountain fault zone does (location constrained by lidar scarps, marked by black, northeast-trending line across lower right of Fig. 1). However, Blakely and others (2009a) also suggest—and appear to favor—the alternative interpretation that these faults do not separate the upper and lower Crescent Formation members in the map area, citing aeromagnetic data and Hirsch and Babcock's (2006) suggestion that the contact between the upper and lower Crescent Formation members represents a separation of metamorphic grade. (See also 'Geologic Setting', above.)

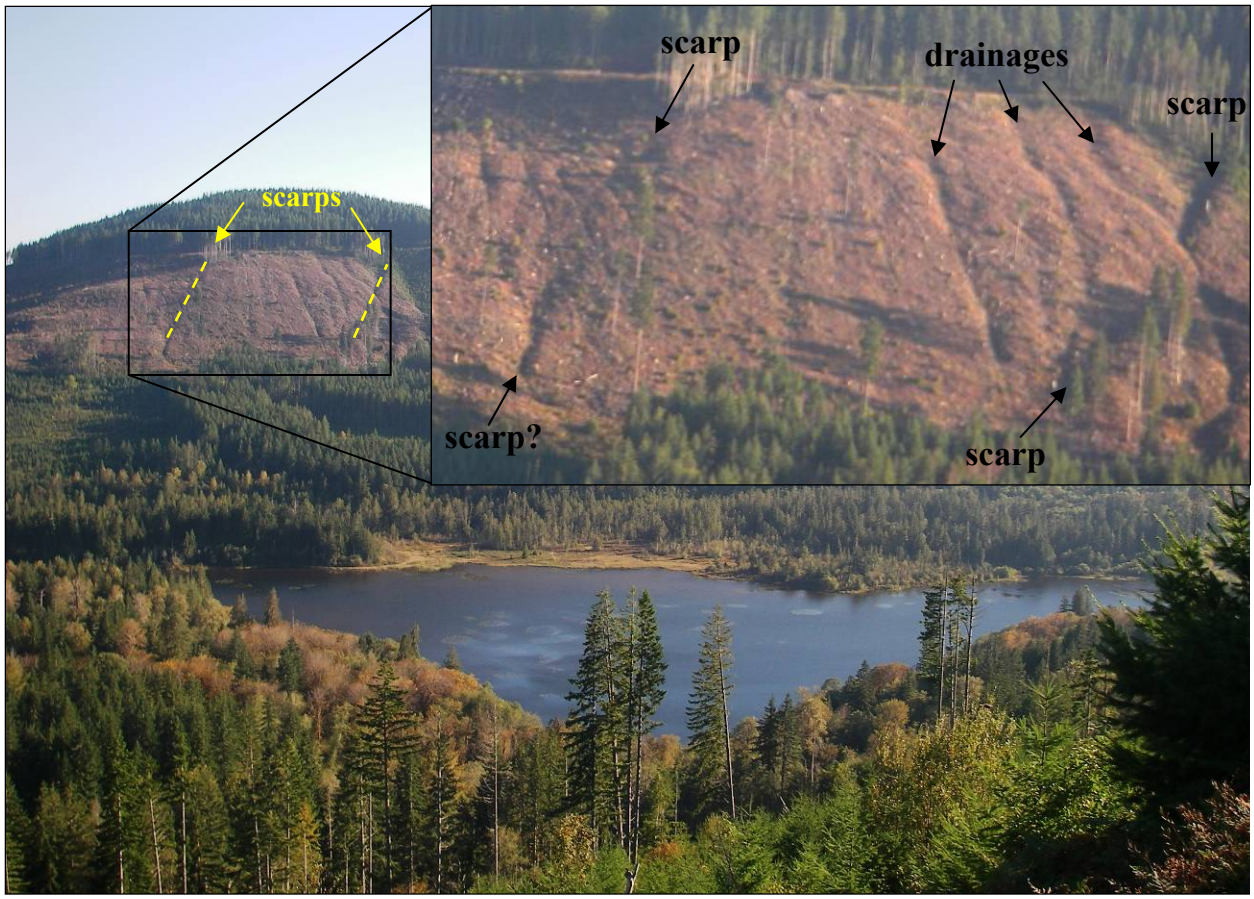

Figure 7. View south from Saddle Mountain across Price Lake to Dow Mountain, where a low sun-angle view of a recent (2010) timber harvest area reveals two north-trending (N10E), west-up scarps (labeled in inset image in upper right and shown as scarp symbols in Polenz and others, 2012) that are oriented oblique to (rotated clockwise away from) drainages. The relation of these scarps to bedrock bedding orientation is not locally constrained by strike and dip measurements, but the regional pattern of bedrock orientations suggests that the scarps could be bedding plane parallel. The scarps are only poorly resolved by the available lidar data. Query at the base of the east scarp indicates that, despite the well-defined appearance of a scarp in this photo, the field impression of the lower sixth of this feature was harder to separate from an artifact of drainage incision. Photos by Michael Polenz.

Blakely and others go on to suggest that the Saddle Mountain fault zone, together with the Frigid Creek and Canyon River faults (both to the southwest), is part of a more than 45 km-long, northeast-trending, sinistral "Saddle Mountain deformation zone" that extends both northeast and southwest of the Hoodsport quadrangle, accommodates northward shortening of Puget Lowland crust relative to the Olympic massif, and is kinematically and spatially linked to the Seattle fault. The notion that the Saddle Mountain fault zone may be linked to a more regional fault system appears consistent with the observation of Babcock and others (1992) that basalts of the Coast Range volcanic province (including Crescent Formation basalt in the map area) are rotated clockwise south of the Bremerton Igneous Complex but lack similar rotation north thereof. Babcock and others (1992) note that the Bremerton Igneous Complex is roughly coincident with the Olympic–Wallowa lineament, which Raisz (1945) and Blakely and others (2009b) associated with a possible fault or fault zone of regional significance.

Hughes (2005), Witter and others (2008), and Blakely and others (2009a) each interpreted the Saddle Mountain fault zone in the vicinity of Price Lake (Fig. 8) as essentially a couplet of southwest-trending faults (the Saddle Mountain East and West faults) that parallel each other and display southeast-up offset (with some component of strike-slip motion). While scarps and trench exposures on both of these faults clearly are southeast-up and this overall pattern may best characterize the Saddle Mountain fault zone around Price Lake, we note several observations that, taken together, suggest that alternate interpretations of the broader fault zone may also merit consideration:

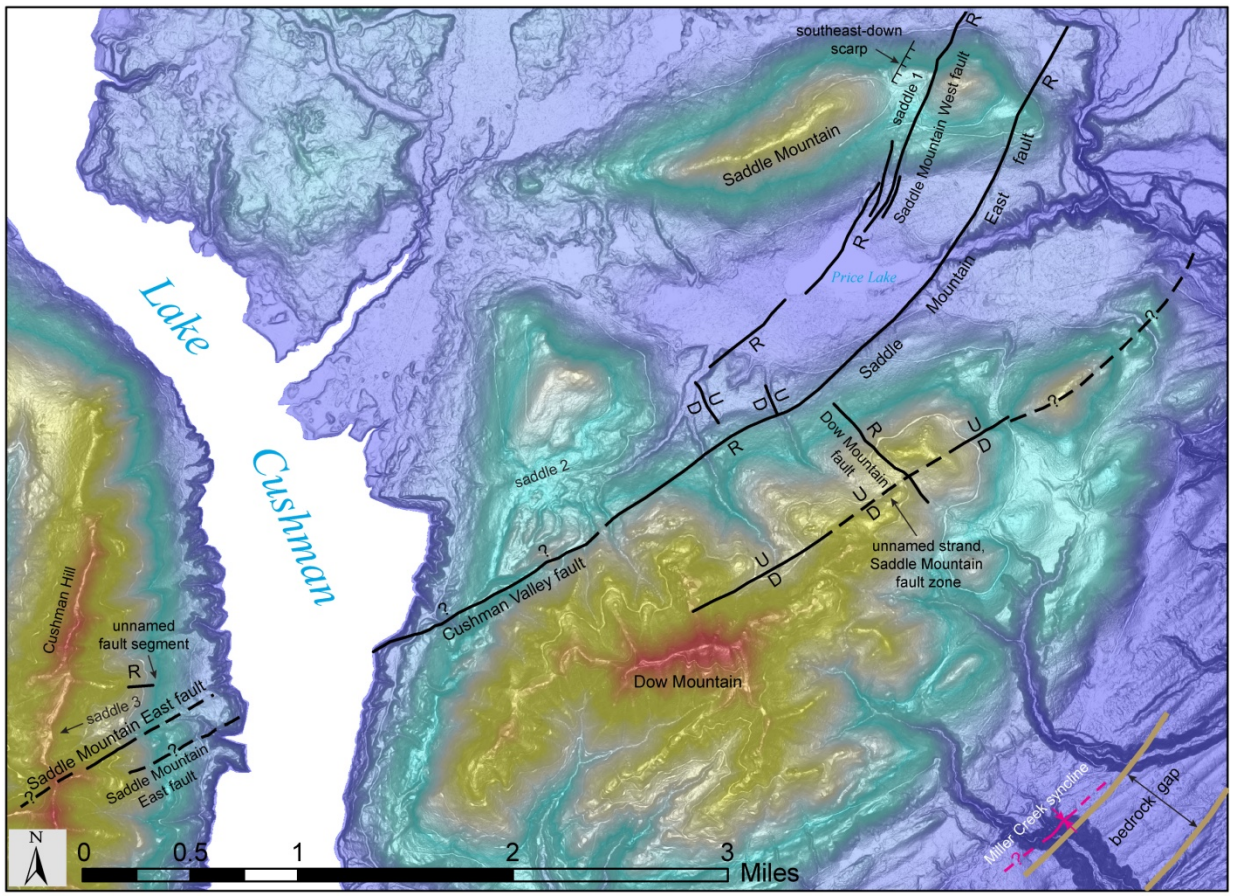

Figure 8. Mapped strands of the Saddle Mountain fault zone in north-central portion of the Hoodsport quadrangle. Not shown but considered part of the Saddle Mountain fault zone are the Frigid Creek and Canyon River faults, both southwest of the image extent. Color serves as proxy for elevation, with darker blue being lowest and red being most elevated. Hillshade image is generated from lidar data with simulated sun angle of 90° and 6 times vertical exaggeration. Features noted are discussed in text above.

1. The fault zone includes multiple southeast-down faults: the Frigid Creek fault (Blakely and others, 2009a; see also discussion [below] of individual structures within the fault zone, and plate in Polenz and others, 2012), and the northeast-trending fault east of the Saddle Mountain East fault (Czajkowski and others, 2009a,b; Blakely and others, 2009a; "unnamed strand, Saddle Mountain fault zone" in Fig. 8, and discussion [below] of individual structures within the fault zone).

2. The apparent northeast-trending bedrock gap southeast of the Miller Creek syncline (lower right corner in Fig. 8) hints at the possible presence of a northeast-trending structural trough, perhaps a graben, northeast of and on trend with the Frigid Creek fault (see also discussion below of the Miller Creek syncline). If real, this trough would add both southeast-down and northwest-down offset along part of the fault zone.

3. On Saddle Mountain west of the Saddle Mountain West fault, a southeast-down scarp ("southeast-down" scarp in Fig. 8; also noted as "unnamed scarp" in fig. 4 of Witter and others, 2008) marks the west side of the saddle that inspired (presumably) the mountain's name.

4. Figure 9 of Blakely and others (2009a) documents a magnetic survey of Price Lake (for location, see upper right of Fig. 8) in which they show three dashed white lines to delineate a magnetic trough on-strike with scarps apparent in lidar. While the easternmost of the three dashed lines is readily interpreted as the southeastern margin of a northeast-trending trough, it is less clear that the dashed lines that mark the northwestern margin of the magnetic trough also represent a northwest-down structure or set of structures as suggested by Witter and others (2008) and Blakely and others (2009a). Alternatively, one might interpret

these western features as southeast-down. If so, then the magnetic trough is bounded on the northwest by a southeast-down feature that could be seen as a southwestern extension of southeast-down offset on the west side of the saddle in Saddle Mountain (see also southeast-down scarp, item 3 above).

5. The saddle on Saddle Mountain is situated northwest of the mapped strands of the Saddle Mountain fault zone ("saddle 1" in upper right of Fig. 8). Similarly, there is a saddle northwest of the mapped strands of the fault zone on the northwest flank of Dow Mountain ("saddle 2" in center of Fig. 8), and the ridge along Cushman Hill is slightly lower north of the mapped strands of the Saddle Mountain fault zone than the ridge farther north or south ("saddle 3" in lower left of Fig. 8). This triplet of saddles, along with the apparent structural trough across Price Lake (see item 4 above), could be the expression of an unrecognized but systematic structural trough marked by southeast-down offset on its northwest side and northwest-down offset on its southeast side.

The above observations suggest that the Saddle Mountain fault zone may be characterized by a combination of structural highs and lows. This may fit into Blakely and others' (2008; 2009a) suggested framework of an en echelon assemblage of faults, but seems to differ from Blakely and others' (2009a) apparent view that southeast-down offset within the fault zone is limited to the southeastern margin of the fault zone. We offer no new insights into the underlying tectonic regime that drives fault motions in the area and provide the above observations only to suggest the possibility of alternative interpretations. The possibility that our observations add up to a meaningful pattern did contribute to the decision to include among the mapped fault strands in Polenz and others (2012) a short, unnamed, east-trending fault segment with apparent north-up offset that we noted along the east slope of Cushman Hill north of the mapped strands of the Saddle Mountain fault ("unnamed fault segment" in Fig. 8). This fault segment was documented at a road cut exposure, where it was marked by multiple subparallel shears with gouge. Field observations on near-vertical slickensides suggest reverse, north-up offset, and we have no evidence for or against post-glacial activity of the strand. The nearly east–west orientation of the segment is rotated somewhat away from the known nearby strands of the Saddle Mountain fault zone and suggests that the strand may be older and unrelated to the Saddle Mountain fault zone.

Post-glacial Tectonic Effects

Post-glacial offset has been demonstrated by eight fault trench investigations within the Saddle Mountain fault zone (http://www.dnr.wa.gov/ResearchScience/Topics/GeosciencesData/Pages/geology_portal.aspx). Six of these trench sites are located in the Hoodsport quadrangle (Carson, 1973; Carson and Wilson, 1974; Wilson, 1975; Witter and others, 2008; Barnett and others, 2009a,b; Czajkowski and others, 2009a,b; Walsh and Logan, 2007—trench on Canyon River fault 11 mi west of the Hoodsport quadrangle; Blakely and others, 2009a—trench on Frigid Creek fault 1,500 ft west of Hoodsport quadrangle). The fault investigations indicate that the Saddle Mountain fault zone produced a M_w 6.5 to 7 earthquake about 1,000 to 1,300 cal yr B.P. (Hughes, 2005; Blakely and others, 2008, 2009a). Although both the Saddle Mountain East and the Saddle Mountain West faults were offset between 1,300 and 1,000 years ago, the radiocarbon data do not permit either separation into separate events or a demonstration of simultaneous offset on the two fault strands, and it therefore remains unproven whether the offset on both faults represents the same event. Witter and others (2008) additionally inferred a prior (smaller?) earthquake on the Saddle Mountain West fault between 17 and 7.7 ka and estimate a post-glacial slip rate between 0.1 and 0.3 mm/yr but note that consideration of just the more recent event makes for a much greater slip rate estimate. They use offset observations from trench exposures to estimate that the two earthquakes produced at least 1 m of southeast-up, vertical separation. This estimate is consistent with the prior estimate of Hughes (2005), who inferred, based on stratigraphic and paleoenvironmental observations other than trench exposures, that between 1,300 and 1,000 years ago, southeast-up reverse dip-slip amounted to 2 m on the Saddle Mountain West fault and 4 m on the Saddle Mountain East fault, thereby reinforcing and refining previous estimates by Wilson and others (1979) of fault rupture timing and slip magnitude based on trench investigations.

Hughes (2005) based his inferences in part on radiocarbon data that he did not individually present in his poster. The individual age analyses are now provided as part of the age-data compilation in Appendix A, and the context for individual analyses is detailed below: Hughes' samples H2a, H3a1, H6a1, H3b1, H3b2, and H9 provide the best estimates for the most recent rupture of the Saddle Mountain East fault strand and are preferable over the dates from H8, H1a, H3a2, and H2b because the former (H2a, etc.) were based on delicate organic matter (conifer needles, cones, leaves, seeds, or other herbaceous structures), whereas the latter were based on wood and charcoal, which would be more likely to survive sedimentary reworking or extended subaerial exposure and thereby could

provide excessively old, inbuilt age estimates (see also Gavin, 2001, on potential significance of inbuilt age). Hughes' (2005) radiocarbon age estimate of Saddle Mountain East fault rupture was based only on samples H3b2 and H9. Hughes analyzed samples H4, H5a, and H5b to constrain movement on the Saddle Mountain West fault by providing a maximum age estimate for submergence of a soil west of that scarp. H5a and H5b are wood fragments from the same stump rooted in the down-dropped soil. While tree rings imply that sample H5a is older than H5b, their ^{14}C age estimates are effectively identical, and due to loss (to weathering) of the outermost tree rings, it is clear that both samples are older than the time of soil submergence, but it remains unknown how much older. Hughes (2005) therefore based his estimate of the timing of Saddle Mountain West fault rupture on sample H4, which dated hemlock needles from the upper end of the submerged soil and therefore should provide a more accurate estimate of the time of subsidence.

The previously mapped structures within the Saddle Mountain fault zone as shown in Polenz and others (2012) were adjusted relative to their equivalent in version 2 of the Washington State Geologic Information Portal to better align with topographic scarps apparent in lidar data. Later editions of the Portal will consider these revisions. Individual faults and their strands are discussed below.

Saddle Mountain East Fault (Including Cushman Rift/Cushman Valley Fault)

The Saddle Mountain East fault alignment shown in Polenz and others (2012) closely resembles that shown by Blakely and others (2009a), although it was adjusted slightly from the Portal along most of its length to better fit lidar scarps. We found no evidence to support a northeastern extension shown by Witter and others (2008) beyond 1,300 ft north of Lilliwaup Creek and therefore, like Blakely and others (2009a), omitted that extension. We also followed Blakely and others (2009a) in not showing a strand across Lilliwaup Creek valley because we saw no expression of the fault in lidar or our field reconnaissance of that area, although we strongly suspect from the presence of scarps north and south of the valley that the fault does cross it. Our identification of a faint, north-trending lineament about 200 ft east of the mapped strands of the Saddle Mountain East fault and seemingly east-up on the north side of the valley (but west-up on the valley floor) suggests that the fault may include more than one strand in this area and contributed to our decision to not connect the strands of the fault that we show north and south of the valley.

Four thousand to 4,500 ft east of Lake Cushman, we dashed the fault where we saw no evidence for its presence in lidar but felt that the Cushman Rift/Cushman Valley fault to the west very likely is part of the Saddle Mountain East fault, as suggested by both Witter and others (2008) and Blakely and others (2009a).

On the east slope of Cushman Hill, the northwestern strand of the Saddle Mountain East fault was extended 0.4 mi to the southwest relative to that fault in the Portal (which was based on Blakely and others, 2009a), thereby nearly connecting with the segment across the hilltop. The extension is weakly supported by lidar landform data but primarily rests on a spectacular forest roadcut exposure at 2,000 ft elevation (Fig. 9). Despite the roadcut exposure, the lidar evidence for all strands of the fault in this area is only faint, and the fault is therefore coded as approximately located except near the roadcut exposure. All strands shown by Blakely and others (2009a) were coded as part of the Saddle Mountain East fault in the Portal, and this label is retained in Polenz and others (2012). However, we caution that we have no compelling reason to reject a connection of at least the northwestern strand(s) to the Saddle Mountain West fault.

Saddle Mountain West Fault

Individual strands of the Saddle Mountain West fault as shown in Polenz and others (2012) are for the most part slightly modified from those shown in the Portal in order to more accurately fit scarps that we observed in lidar data. One strand of the Saddle Mountain West fault north of Price Lake was shifted slightly eastward, lengthened slightly at its northern end, and, consistent with the analysis of Hughes (2005) and dashed line suggestions of Witter and others (2008) and Blakely and others (2009a), extended at the south end to cross Price Lake where aerial photographs reveal a submerged southeast-up scarp. While it is clear that a scarp is present beneath the lake, it is less clear which (if any) of the strands to the northeast connects with it. The strand we chose best fits with the combined lidar and 2009 and earlier aerial photographic images available to us, but it is possible that a more easterly strand connects to the submerged scarp beneath Price Lake. The northwestern strand shown by Witter and others (2008) and Blakely and others (2009a) across the saddle of Saddle Mountain was shortened in Polenz and others (2012) because we saw no evidence for it atop the saddle. On the south-facing slope of Saddle Mountain, our consideration of lidar data suggests that the strand is east-up, but if it were extended across the saddle, the topography atop the saddle would suggest west-up offset. In addition, a southeast-down scarp that runs down the

north-facing slope of the mountain ("southeast-down scarp" at top of Fig. 8, also noted by Witter and others, 2008) would appear to be the direct extension of this strand. We therefore opted in Polenz and others (2012) to truncate the strand where we cease to see its northern extension in the lidar data and separately showed a west-up scarp (not coded as fault but probably most easily explained as fault strand) down the north face of the mountain (see also Fig. 8).

Figure 9. Crescent Formation basalt (pillowed in center) with multiple shear planes interpreted as likely Saddle Mountain East fault strand exposures. Note the offset pillow structures along the prominent shear plane (upper right to lower left) across the center of the image. View to southwest. Photo by Michael Polenz.

Dow Mountain Fault

The Dow Mountain fault was first documented by Carson and Wilson (1974) along a northwest-trending scarp that traverses the northeastern flank of Dow Mountain. They describe the fault based on initial evidence from a northwest-trending photogrammetric lineament associated with a southwest-facing scarp as much as 35 ft high, although Wilson and others (1979) note a lesser 26 ft scarp height. Trench data revealed reverse offset on a fault plane dipping 59° northeast (Fig. 10; Carson and Wilson, 1974; Wilson and others, 1979; significant site DMFT in Polenz and others, 2012).

Carson and Wilson (1974) and Wilson and others (1979) interpreted the last major movement on the Dow Mountain fault to be pre-Vashon in age, based on their sense that the fault trench exposure does not offset Vashon Drift. However, the mere fact that the Dow Mountain fault has a surface expression seen easily on air photos suggests that it is post-Vashon, and lidar data show the scarp offsetting the surface in areas mapped by Polenz and others (2012) as Vashon-age till. Yet Polenz and others' (2012) field data-point density in these areas was limited, and some deposits that they interpreted as Vashon till would fit Wilson and others' (1979) description of pre-Vashon till: "fresh clasts with clay skins and a matrix oxidized to a reddish-brown color". Consequently, we favor the notion that the Dow Mountain fault has been post-glacially active, but the interpretation remains unproven. The Dow Mountain fault may be offset by the Saddle Mountain East fault (Carson and Wilson, 1974).

Figure 10. View to southeast of the Dow Mountain fault (from notebook in lower center to upper right corner). The northeast-dipping structure elevated the basalt bedrock on the left (northeast) over Quaternary sediment on the right (southwest). Inset in upper left shows view down the trench. Photos by Robert Carson.

In Polenz and others (2012), we adjusted the location of the Dow Mountain fault slightly to better conform to lidar-identified scarps, shifting the fault slightly to the southwest. The scarp ranges from poorly expressed to clearly apparent in lidar data, and we show the fault along 3,500 ft of the scarp. Based purely on consideration of lidar data, one might extend the fault another 150 ft to the southeast. We did not do so in Polenz and others (2012) because the evidence for this extension is ambiguous and our field data did not provide constraining data.

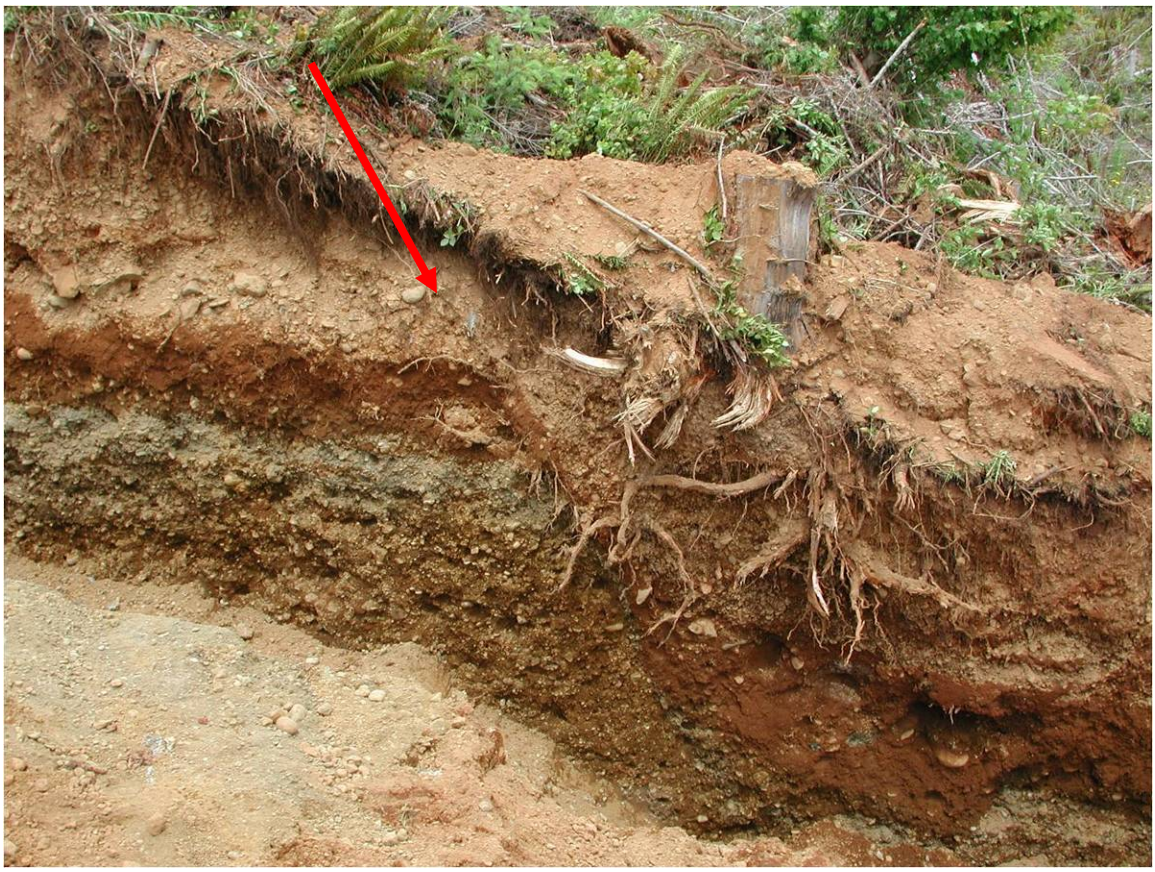

Figure 11. East-northeast view of Frigid Creek fault investigation trench exposure 1,500 ft west of the map area. Red arrow points at southeast-down shear surface. Photo by Tim Walsh.

Frigid Creek Fault

A northeast-trending "Frigid Creek scarp"(s) was shown by Witter and Givler (2005) and Witter and others (2008). In their conclusions, Witter and others (2008) referred to the "Frigid Creek fault" and its "inferred connection" to the Saddle Mountain fault based on regional aeromagnetic data. Blakely and others (2009a) illustrate fault trench data from 1,500 ft west of the map area and interpret the trench exposure (Fig. 11) and a set of southeast-down, distinct lidar scarps that extend east into the map area as evidence for south-down normal faulting and "expect" a component of sinistral slip because they interpret the fault as kinetically linked to the Saddle Mountain fault zone and the Seattle fault. The trench exposure yielded evidence for at least one post-glacial event between 5,657 and 319 cal yr B.P. (Blakely and others, 2009a; Appendix A) and could be interpreted as landslide offset. However, even if the displacement in the trench represents landslide motion, a tectonic link appears reasonable because the trench exposure is associated with a 2 mi-long set of linear, south(east)-down scarps along the base of and parallel to a strikingly linear south(east)-facing mountain front, and Blakely and others (2009a) show that within the map area, most of this topography coincides with a sharp magnetic anomaly. However, Blakely and others (2009a) interpret that anomaly as a fold in Crescent Formation basalt and speculate that the fault is only shallow. The strands of the Frigid Creek fault shown in this map are modified after Blakely and others (2009a) to better align strands with topographic scarps apparent in lidar data. Segments for which we did not see scarps are coded as inferred, and all segments are queried because all evidence we are aware of permits interpretation of the fault as essentially a set of landslide scarps, although there is no corresponding evidence for downslope landslide-related deformation or landslide deposits. We added a cluster of scarps and lineaments aligned with and near the mapped fault strands. These unexplained features may merit further consideration but have not been shown to be tectonic. We additionally speculate that the newly documented Miller Creek syncline (discussion below, and Polenz

Figure 12. View to southwest of “Alligator trench” exposing the unnamed fault east of the Saddle Mountain East fault. The fault is marked by the near-vertical line of red flags across the center of the image and has elevated basalt bedrock on the right (northwest) relative to Quaternary sediment on the left (southeast). Photo by Tim Walsh.

and others, 2012) may be evidence that the Frigid Creek fault extends farther northeast than previously mapped by Blakely and others (2009a).

Unnamed Fault East of the Saddle Mountain East Fault

A southwest-trending, northwest-up scarp runs approximately 3,000 ft southeast of and parallel to the Saddle Mountain East fault ("unnamed strand, Saddle Mountain fault zone" in center-right of Fig. 8). Blakely and others (2009a) showed this lidar-identified scarp as a solid line northeast of the Dow Mountain fault and as dashed scarp west of the Dow Mountain fault. Witter and others (2008) had drawn it as a solid line on both sides of the Dow Mountain fault. Czajkowski and others (2009a,b) trenched the scarp 1,900 ft east of the Dow Mountain fault (significant site AT in Polenz and others, 2012) and found "strong evidence for multiple (possibly four) Holocene-age faulting events" on a steeply northwest-dipping fault (Fig. 12). The scarp is therefore presented as a definite fault strand here (Fig. 8, dashed where approximately located) and in Polenz and others (2012). Barnett and others (2009b) provided radiocarbon age control on a ground-rupturing earthquake recorded in this trench 1,330 to 1,260 cal yr B.P. and a possible earlier rupture 3,700 to 3,480 cal yr B.P. Slightly revised (due to use of updated calibration software, Elizabeth Barnett, USGS, written commun., 2010) two-sigma ^{14}C age estimates and previously unpublished sample details for both dates are presented in Appendix A.

Witter and others (2008) and Blakely and others (2009a) terminated the scarp approximately 2,500 ft northeast of the Dow Mountain fault. We believe that discontinuous and faint lidar-scarp segments, ridge-top depressions, rock fall deposits 6,700 ft northeast of the Dow Mountain fault, and landslides elsewhere along the apparent fault support an extension of the same fault by at least 6,500 ft farther northeast (dashed and queried fault in center-east of Fig. 8; Polenz and others, 2012). Just northeast of the end point of this apparent fault segment, a lineament across Lilliwaup Creek valley marks a set of kinks that add up to a 0.2- to 0.5-mi left step in that valley. These kinks and a nearby Lilliwaup Creek knickpoint where lidar data shows an approximately 20-ft drop in the channel bed suggest that the putative fault may extend farther northeast across Lilliwaup Creek.

Other Unnamed Faults

Two northwest-trending, southwest-facing scarp segments 0.25 and 0.5 mi west of and subparallel to the northwest end of the Dow Mountain fault were adjusted slightly in Fig. 8 and in Polenz and others (2012) (relative to their equivalents in Witter and others, 2008; Blakely and others, 2009a; and the Portal, v. 2), to better fit lidar data. A short, east-trending fault strand ("unnamed fault strand" on east face of Cushman Hill in Fig. 8; also shown across geochemical data site and age location CHU in Polenz and others, 2012) is rotated slightly away from the alignment of nearby strands of the Saddle Mountain East fault and is discussed in the general discussion of the Saddle Mountain fault zone (above).

Miller Creek Syncline

Along a segment of Miller Creek southeast of Dow Mountain (1 mi west of the eastern map edge in Polenz and others, 2012), rhythmite beds of unit ΦEm, which otherwise display consistent southeast dips, are marked by a concave-up, gentle, northeast-trending, parallel fold (informally named "Miller Creek syncline" in Polenz and others, 2012) that changes bedding orientations over a distance of no more than 15 ft from the typical, steeply (53°) southeast dipping orientation of the northwest limb (Figs. 13A,B) to a gently undulating and roughly horizontal southeast limb (Fig. 13C). The near-level beds in the southeast limb (Fig. 13A) imply that folding rotated the deposits in the syncline's southeast limb by at least about 50 degrees about a subhorizontal axis to achieve the level bedding there. Farther southeast along the adjacent 250 ft of channel length, the southeast limb is discontinuously exposed but eventually dips gently (18°) northwest before bedrock exposures are truncated by a near-vertical contact against Quaternary deposits (unit Qga). The exposed face of this contact is 30 ft high, but about 300 ft to the west (at the northwest side of the fold), the southern valley wall exposes at least 150 ft of bedrock, thus suggesting a steep contact of similar height where the bedrock ends. No deformation was observed in the Quaternary deposits, but exposures were limited, and deformation could thus have been missed.

The steep contact between the sedimentary bedrock and the Quaternary sediment southeast of the Miller Creek syncline marks the beginning of 0.5 mi of Quaternary exposures. East of the Quaternary exposures, sedimentary bedrock (also mapped as unit ΦEm) again emerges and abruptly rises up approximately 160 ft along another near-vertical contact. Such a strikingly steep-walled gap in sedimentary bedrock exposures was not observed elsewhere. There is, however, a 0.5 mi gap in bedrock along Sund Creek (0.5–1 mi north of Miller Creek), which suggests a bedrock trough that parallels the Miller Creek syncline and Hood Canal. The fate of this trough southwest

of Miller Creek is unclear, but a rise in the upland surface elevation about 0.3 mi southeast of Miller Creek suggests a possible termination of the trough there.

Figure 13. A. View to southwest of southeast-dipping rhythmite beds of unit ΦEm northwest of the Miller Creek syncline. The steep gorge upvalley of the syncline is marked by a series of waterfalls, some estimated at close to 30 ft high. The one pictured is less than 10 ft high. **B.** Close-up view of southeast-dipping rhythmite beds of unit ΦEm northwest of Miller Creek syncline. Coarser, pale gray beds on left are upsection of brown, weathered but otherwise similar beds in lower right. Brendan Miller is crouching upright. **C.** View to northeast of gently undulating, nearly level rhythmite beds of unit ΦEm in southeast limb of Miller Creek syncline. Photos by Michael Polenz.

Where unit ΦEm bedrock exposures resume east of the 0.5 mi bedrock gap, beds strike north-northwest (345°) and dip northeast (42°). Additional exposures of unit ΦEm 0.5 mi farther east (at the east edge of the Hoodsport quadrangle) strike northeast (35°) and dip southeast (60°), consistent with regional trends and thus resuming the bedding orientations that define the northwest limb of the Miller Creek syncline and also generally prevail northwest of the syncline. This implies that the Miller Creek syncline is only part of a larger structure or set of structures, the simplest interpretation being a structural terrace, although the bedrock trough and the aberrant bedding orientation (345°/42°) at its southeastern edge suggest more complexity, perhaps a graben related to the Saddle Mountain fault zone.

The structural context of the Miller Creek syncline is thus unresolved. It may be worth noting, however, that the observed syncline, like the Frigid Creek fault, is located 2.4 mi southeast of and subparallel to the Saddle Mountain East fault. This suggests that the Miller Creek syncline and the Frigid Creek fault may be kinematically linked.

OTHER STRUCTURES

Lucky Dog Structure

The Lucky Dog structure is an apparent Holocene-active, northwest-trending, shallow-crustal reverse fault or anticline north of and in the Skokomish valley (Polenz and others, 2010a,b) 2 mi south of the map area. Our mapping did not reveal firm evidence for (or against) a northwest extension of this fault, but we noted a few features that suggest a possible northwest extension.

Aeromagnetic data (Blakely and others, 2009a) reveal three northwest-trending lineaments along which magnetic field strength in each case decreases northeast. The three lineaments run roughly perpendicular to the Frigid Creek fault and are best expressed within 1 to 2 mi of it. The southwesternmost of the three is the weakest and forms a concave-west arc roughly along the alignment of an unnamed, north-trending, concave-west branch of Frigid Creek. The two others are 0.5 to 2 mi farther northeast. The central of the three lineaments roughly parallels McTaggert Creek, running about 1,500 to 3,000 ft east of the creek. The southwestern and central lineaments seem to approximately bracket what could be a northwest extension of Polenz and others' (2010a,b) Lucky Dog structure. The northeastern lineament is the straightest and strongest of the three, and it roughly (and tortuously) aligns with Lake Kokanee away from the Frigid Creek fault before straightening out and continuing southeast along the course of the water pipeline that carries Lake Kokanee water to Tacoma Power's hydropower plant at Potlatch south of the Hoodsport quadrangle. It thereby trends towards an offshore location where Polenz and others (2010a,b) were not able to gather structural data.

We noted steeply west- to south-dipping, pre-Fraser Quaternary beds along McTaggert Creek (see attitude measurements on map, Polenz and others, 2012), a possible structural equivalent of those along the southwestern edge of the Lucky Dog structure noted by Polenz and others (2010a,b) and situated between the westernmost and central of the three magnetic lineaments. Strata along Frigid Creek also display some aberrant dips, but their orientations are more diverse and do not seem to add up to a coherent pattern, whereas a southwest-down pattern is at least loosely apparent among the dips along McTaggert Creek. The varied dips along Frigid Creek may in part be a function of the relatively advanced sedimentary age, with the section there being generally magnetically reversed. No age-control data are available for the southwest-dipping beds along McTaggert Creek.

East of McTaggert Creek, the central and eastern of the three lineaments bracket an apparent belt of shallow (Crescent Formation) bedrock, with exposure reaching up to 500 ft elevation. East of the eastern magnetic lineament, bedrock seems to be about 100 to 150 ft lower, at roughly 350 to 400 ft elevation (see cross section A in Polenz and others, 2012), and a geomagnetic depression southeast of Lake Kokanee reinforces the sense of a likely bedrock low. To the west, neither McTaggert Creek nor Frigid Creek offer bedrock exposures within the map area.

Finally, we noted that a cluster of large, morphologically distinct landslides along a set of meander bends of the North Fork Skokomish River is located just east of the alignment of the central magnetic lineament. To the extent that these landslides may be active, they are not likely related to undercutting along the North Fork Skokomish River channel because that channel is entrenched in bedrock, and the landslides seem to rest upslope thereof. They are, however, most distinctive in (and may be limited to) the outer bends of the valley thus occupying convergent slopes in Quaternary sediment. Whether and in what manner these slides may be related to a possible northwest extension of the Lucky Dog structure into the Hoodsport 7.5 minute quadrangle remains unresolved. We note here only their coincident presence as one of several possible attributes alongside magnetic anomalies, elevated bedrock, and unusual but systematically south- to west-dipping Quaternary beds. All of these features could reasonably be associated with the northwest extension of a northwest-trending structure that has elevated the center of its trend where Polenz and others (2010a,b) documented the structure southeast of the Hoodsport quadrangle. However, these coincidences are far from compelling, and a well-informed judgment about a possible northwest extension of the Lucky Dog structure therefore must await further study. Analysis of magnetic data to concentrate on shallow structures (which proved vital in recognizing the geomagnetic signature of the structure in the Skokomish Valley), especially if coupled with improved gravity surveying and a targeted field investigation, may shed additional light on the issue. Such efforts seem merited given the considerable magnitude of late Holocene valley floor deformation associated with the Lucky Dog structure in the Skokomish Valley, and the proximity of the structure to critical infrastructure of the Skokomish Tribe, as well as two dams on the North Fork Skokomish River.

Hood Canal Fault

Our geological mapping produced no data regarding the existence or character of the Hood Canal fault, and we copied the structure from the Portal. The putative fault was suggested (but not named) by Daneš and others (1965)

based on analysis of surface geology, gravity, and magnetic data. Yount and others (1985) and Gower and others (1985) similarly used geophysical data in support of an unnamed probable fault. Dragovich and others (2002) coded the putative fault as concealed and referred to it as Hood Canal fault. Haug (1998) presents interpretations of numerous high-resolution seismic line data that consistently show the Hood Canal fault. In contrast, Richard Blakely (written commun., 2008) and Lamb and others (2009) use magnetic data and recent models to cast doubt on the existence of the fault, citing the lack of a magnetic anomaly where Crescent Formation basalt, if offset, should produce an anomaly. Contreras and others (2010) noted that an apparent vertical offset (in their cross section) across Hood Canal east of the Hoodsport quadrangle is likely an artifact of poorly constrained contacts. Additional discussion of the postulated fault is provided by Lidke (2003a).

ACKNOWLEDGMENTS

The geologic mapping discussed in this report was funded in part by the U.S. Geological Survey National Cooperative Geologic Mapping Program under award no. G10AC00363. We thank Mason County for assisting our mapping with GIS data; Eric Schuster (DGER) and Kathleen Hawes (South Puget Sound Community College) for assistance with wood sample processing and analysis; the U.S. Geological Survey Mendenhall Postdoctoral Fellowship program for funding field activities and radiocarbon analyses by Jonathan Hughes; Elizabeth Barnett (USGS), Brian Sherrod (USGS), and Robert Witter (Oregon Dept. of Geology and Mineral Industries) for supplying, verifying, and (or) permitting publication of ^{14}C data and (or) related sample details, especially where previously unpublished; Richard Blakely (USGS) for aeromagnetic data and assistance with its interpretation; Megan Anderson (Colorado College) for assisting with interpretation of geophysical data; Elizabeth Nesbitt (Univ. of Wash./Burke Museum of Paleontology) for assistance with processing and stratigraphic interpretation of sedimentary rocks; Glenn Thackray and Wendy Gerstel for their insights into the record of glaciations of the Olympic Mountains; Joe Dragovich, Trevor Contreras, and Jessica Czajkowski (all DGER) and Rowland Tabor (USGS) for reviews and assistance with interpretation of aspects of this mapping; Tacoma Power for assisting with land access, field logistics, and proprietary geologic records; Steve Brown and the employees of Trout Lodge, LLC, and Dannie and Patricia Lewallen for land access, boring records, and assistance with determining accurate boring site locations; Green Diamond Resource Co., Manke Lumber Co., Green Crow Corp., the U.S. Forest Service, Tim Sheldon, Jim Goodpaster, Brian Sund, and uncounted other landowners for permitting us to map on their land and providing valuable local knowledge.

REFERENCES CITED

Atwater, B. F., 1999, Radiocarbon dating of a Seattle earthquake to A.D. 900-930 [abstract]: Seismological Research Letters, v. 70, no. 2, p. 232.

Babcock, R. S.; Burmester, R. F.; Engebretson, D. C.; Warnock, A. C.; Clark, K. P., 1992, A rifted margin origin for the Crescent basalts and related rocks in the northern Coast Range volcanic province, Washington and British Columbia: Journal of Geophysical Research, v. 97, no. B5, p. 6799-6821.

Babcock, R. S.; Suczek, C. A.; Engebretson, D. C., 1994, The Crescent "terrane", Olympic Peninsula and southern Vancouver Island. *In* Lasmanis, Raymond; Cheney, E. S., convenors, Regional geology of Washington State: Washington Division of Geology and Earth Resources Bulletin 80, p. 141-157. [http://www.dnr.wa.gov/Publications/ger_b80_regional_geol_wa_2.pdf]

Barnett, E. A.; Sherrod, B. L.; Kelsey, H. M.; Czajkowski, J. L.; Walsh, T. J.; Contreras, T. A.; Davis-Staunton [*sic*: Davis-Stanton; spelling corrected on poster], K.; Schermer, E. R.; Carson, R. J., 2009a, Active faulting along the Saddle Mountain fault zone, southeast Olympic Mountains, WA [abstract]: Eos (American Geophysical Union Transactions), v. 90, no. 52, Suppl. S51B-1404.

Barnett, E. A.; Sherrod, B. L.; Kelsey, H. M.; Czajkowski, J. L.; Walsh, T. J.; Contreras, T. A.; Davis-Stanton, K.; Schermer, E. R.; Carson, R. J., 2009b, [poster for] Active faulting along the Saddle Mountain fault zone, southeast Olympic Mountains, WA [abstract]: Eos (American Geophysical Union Transactions), v. 90, no. 52, Suppl. S51B-1404.

Birdseye, R. U.; Carson, R. J., 1989, Tephra of Salmon Springs age from the southeastern Olympic Peninsula, Washington: Washington Division of Geology and Earth Resources Open File Report 74-1 (revised), 23 p. [http://www.dnr.wa.gov/publications/ger_ofr74-1_tephra_olympic_peninsula.pdf]

Blakely, R. J.; Sherrod, B. L.; Hughes, J. F.; Anderson, M. L.; Wells, R. E.; Weaver, C. S., 2008, Western boundary of the Seattle uplift, Washington [abstract]: Eos (American Geophysical Union Transactions), v. 89, no. 53, Suppl., p. F2481.

Blakely, R. J.; Sherrod, B. L.; Hughes, J. F.; Anderson, M. L.; Wells, R. E.; Weaver, C. S., 2009a, Saddle Mountain fault deformation zone, Olympic Peninsula, Washington—Western boundary of the Seattle uplift: Geosphere, v. 5, no. 2, p. 105-125.

Blakely, R. J.; Sherrod, B. L.; Weaver, C. S.; Wells, R. E., 2009b, Connecting crustal faults and tectonics from Puget Sound across the Cascade Range to the Yakima fold and thrust belt, Washington—Evidence from new high-resolution aeromagnetic data [abstract]: Eos (American Geophysical Union Transactions), v. 90, no. 22, p. JA203-JA204.

Booth, D. B.; Troost, K. G.; Clague, J. J.; Waitt, R. B., 2004, The Cordilleran ice sheet. *In* Gillespie, A. R.; Porter, S. C.; Atwater, B. F., editors, The Quaternary period in the United States: Elsevier, p. 17-43.

Borchardt, G. A.; Aruscavage, P. J.; Millard, H. T., Jr., 1972, Correlation of the Bishop ash, a Pleistocene marker bed, using instrumental neutron activation analysis: Journal of Sedimentary Petrology, v. 42, no. 2, p. 301-306.

Bretz, J H., 1913, Glaciation of the Puget Sound region: Washington Geological Survey Bulletin 8, 244 p., 3 plates. [http://www.dnr.wa.gov/publications/ger_b8_glaciation_pugetsound.pdf]

Brocher, T. M.; Parsons, T. E.; Blakely, R. J.; Christensen, N. I.; Fisher, M. A.; Wells, R. E.; SHIPS Working Group, 2001, Upper crustal structure in Puget Lowland, Washington—Results from the 1998 Seismic Hazards Investigations in Puget Sound: Journal of Geophysical Research, v. 106, no. B7, p. 13,541-13,564.

Brown, E. H.; Dragovich, J. D., 2003, Tectonic elements and evolution of northwest Washington: Washington Division of Geology and Earth Resources Geologic Map GM-52, 1 sheet, scale 1:625,000, with 12 p. text. [http://www.dnr.wa.gov/Publications/ger_gm52_tectonic_evolution_nw_washington.zip]

Carson, R. J., 1973, First known active fault in Washington: Washington Geologic Newsletter, v. 1, no. 3, p. 1-2. [http://www.dnr.wa.gov/Publications/ger_washington_geology_1973_v1_no3.pdf]

Carson, R. J., 1976, Geologic map of north-central Mason County, Washington: Washington Division of Geology and Earth Resources Open File Report 76-2, 1 sheet, scale 1:62,500. [http://www.dnr.wa.gov/Publications/ger_ofr76-2_geol_map_mason_co_62k.pdf]

Carson, R. J., 1979, Reinterpretation of the Skokomish gravel, southwestern Puget Lowland, Washington [abstract]: Northwest Scientific Association, Annual Meeting, 52nd, Program and Abstracts, p. 31.

Carson, R. J., 1980, Quaternary, environmental, and economic geology of the eastern Olympic Peninsula, Washington: [unpublished report], 275 p.

Carson, R. J.; Wilson, J. R., 1974, Quaternary faulting on Dow Mountain, Mason County: Washington Geologic Newsletter, v. 2, no. 4, p. 9-10. [http://www.dnr.wa.gov/Publications/ger_washington_geology_1974_v2_no4.pdf]

Contreras, T. A.; Legorreta Paulin, Gabriel; Czajkowski, J. L.; Polenz, Michael; Logan, R. L.; Carson, R. J.; Mahan, S. A.; Walsh, T. J.; Johnson, C. N.; Skov, R. H., 2010, Geologic map of the Lilliwaup 7.5-minute quadrangle, Mason County, Washington: Washington Division of Geology and Earth Resources Open File Report 2010-4, 13 p., 1 plate, scale 1:24,000. [http://www.dnr.wa.gov/Publications/ger_ofr2010-4_geol_map_lilliwaup_24k.zip]

Czajkowski, J. L.; Walsh, T. J.; Contreras, T. A.; Davis-Stanton, Kelsay; Kelsey, H. M.; Schermer, E. R.; Carson, R. J., 2009a, Active faulting along a newly-found segment of the Saddle Mountain fault zone, southeastern Olympic Mountains, WA—A paleoseismic trenching study [abstract]: Geological Society of America Abstracts with Programs, v. 41, no. 7, p. 479.

Czajkowski, J. L.; Walsh, T. J.; Contreras, T. A.; Davis-Stanton, Kelsay; Kelsey, H. M.; Schermer, E. R.; Carson, R. J., 2009b, Active faulting along a segment of the Saddle Mountain fault zone, southeastern Olympic Mountains, WA—A paleoseismic trenching study [abstract]. *In* Northwest Scientific Association, The Pacific Northwest in a changing environment—Northwest Scientific Association 81st annual meeting; Program with abstracts: Northwest Scientific Association, p. 14.

Daneš, Z. F.; Bonno, M.; Brau, J. E.; Gilham, W. D.; Hoffman, T. F.; Johansen, D.; Jones, M. H.; Malfait, Bruce; Masten, J.; Teague, G. O., 1965, Geophysical investigation of the southern Puget Sound area, Washington: Journal of Geophysical Research, v. 70, no. 22, p. 5573-5580.

Derkey, R. E.; Heheman, N. J.; Alldritt, Katelin, 2009a, Geologic map of the Lake Wooten 7.5-minute quadrangle, Mason County, Washington: Washington Division of Geology and Earth Resources Open File Report 2009-5, 1 sheet, scale 1:24,000. [http://www.dnr.wa.gov/Publications/ger_ofr2009-5_geol_map_lakewooten_24k.pdf]

Derkey, R. E.; Heheman, N. J.; Alldritt, Katelin, 2009b, Geologic map of the Mason Lake 7.5-minute quadrangle, Mason County, Washington: Washington Division of Geology and Earth Resources Open File Report 2009-6, 1 sheet, scale 1:24,000. [http://www.dnr.wa.gov/Publications/ger_ofr2009-6_geol_map_masonlake_24k.pdf]

Dragovich, J. D.; Logan, R. L.; Schasse, H. W.; Walsh, T. J.; Lingley, W. S., Jr.; Norman, D. K.; Gerstel, W. J.; Lapen, T. J.; Schuster, J. E.; Meyers, K. D., 2002, Geologic map of Washington—Northwest quadrant: Washington Division of Geology and Earth Resources Geologic Map GM-50, 3 sheets, scale 1:250,000, with 72 p. text. [http://www.dnr.wa.gov/publications/ger_gm50_geol_map_nw_wa_250k.pdf]

Easterbrook, D. J.; Roland, J. L.; Carson, R. J.; Naeser, N. D., 1988, Application of paleomagnetism, fission-track dating, and tephra correlation to lower Pleistocene sediments in the Puget Lowland, Washington. *In* Easterbrook, D. J., editor, Dating Quaternary sediments: Geological Society of America Special Paper 227, p. 139-165.

Foit, F. F., Jr.; Gavin, D. G.; Hu, F. S., 2004, The tephra stratigraphy of two lakes in south-central British Columbia, Canada and its implications for mid-late Holocene volcanic activity at Glacier Peak and Mount St. Helens, Washington, USA: Canadian Journal of Earth Sciences, v. 41, no. 12, p. 1401-1410.

Gavin, D. G., 2001, Estimation of inbuilt age in radiocarbon ages of soil charcoal for fire history studies: Radiocarbon, v. 43, no. 1, p. 27-44.

Glassley, W. E., 1974, Geochemistry and tectonics of the Crescent volcanic rocks, Olympic Peninsula, Washington: Geological Society of America Bulletin, v. 85, no. 5, p. 785-794.

Gower, H. D.; Yount, J. C.; Crosson, R. S., 1985, Seismotectonic map of the Puget Sound region, Washington: U.S. Geological Survey Miscellaneous Investigations Series Map I-1613, 1 sheet, scale 1:250,000, with 15 p. text.

Hallet, D. J.; Hills, L. V.; Clague, J. J., 1997, New accelerator mass spectrometry radiocarbon ages for the Mazama tephra layer from Kootenay National Park, British Columbia, Canada: Canadian Journal of Earth Sciences, v. 34, p. 1202-1209.

Haug, B. J., 1998, High resolution seismic reflection interpretations of the Hood Canal–Discovery Bay fault zone; Puget Sound, Washington: Portland State University Master of Science thesis, 1 v.

Haugerud, R. A., 2005, Preliminary geologic map of Bainbridge Island, Washington: U.S. Geological Survey Open-File Report 2005-1387, version 1.0, 1 sheet, scale 1:24,000. [http://pubs.usgs.gov/of/2005/1387/]

Haugerud, R. A., 2009, Preliminary geomorphic map of the Kitsap Peninsula, Washington; version 1.0: U.S. Geological Survey Open-File Report 2009-1033, 2 sheets, scale 1:36,000. [http://pubs.usgs.gov/of/2009/1033/]

Hirsch, D. M.; Babcock, Scott, 2006, Unexpected vertical variations in metamorphism within the Crescent basalt, Dosewallips River valley, Olympic Peninsula, Washington State [abstract]: Geological Society of America Abstracts with Programs, v. 38, no. 5, p. 18.

Hirsch, D. M.; Babcock, R. S., 2009, Spatially heterogeneous burial and high-P/T metamorphism in the Crescent Formation, Olympic Peninsula, Washington: American Mineralogist, v. 94, no. 8-9, p. 1103-1110.

Hughes, J. F., 2005, Meters of synchronous Holocene slip on two strands of a fault in the western Puget Sound Lowland, Washington [abstract]: Eos (American Geophysical Union Transactions), v. 86, no. 52, p. F1437.

Johnson, S. Y.; Blakely, R. J.; Stephenson, W. J.; Dadisman, S. V.; Fisher, M. A., 2004, Active shortening of the Cascadia forearc and implications for seismic hazards of the Puget Lowland: Tectonics, v. 23, TC1011, doi:10.1029/2003TC001507, 2004, 27 p.

Koppers, A. A. P.; Staudigel, Hubert; Duncan, R. A., 2003, High-resolution $^{40}Ar/^{39}Ar$ dating of the oldest oceanic basement basalts in the western Pacific basin: Geochemistry Geophysics Geosystems, v. 4, no. 11, 20 p.

Lamb, A. P.; Liberty, L. M.; Blakely, R. J.; Van Wijk, Kasper, 2009, The Tahuya lineament—Southwestern extension of the Seattle fault? [abstract]: Geological Society of America Abstracts with Programs, v. 41, no. 7, p. 479.

Lidke, D. J., compiler, 2003a, Fault number 552, Hood Canal fault zone. *In* U.S. Geological Survey, Quaternary fault and fold database of the United States: U.S. Geological Survey website [accessed Aug. 6, 2010, at http://geohazards.usgs.gov/cfusion/qfault/qf_web_disp.cfm?qfault_or=2522&ims_cf_cd=cf&disp_cd=C].

Lidke, D. J., compiler, 2003b, Fault number 575, Saddle Mountain Faults. *In* U.S. Geological Survey, Quaternary fault and fold database of the United States: U.S. Geological Survey website [accessed Aug. 6, 2010 at http://earthquake.usgs.gov/hazards/qfaults/; http://geohazards.usgs.gov/cfusion/qfault/qf_web_disp.cfm?qfault_or=1345&ims_cf_cd=cf&disp_cd=C].

Logan, R. L., 2003, Geologic map of the Shelton 1:100,000 quadrangle, Washington: Washington Division of Geology and Earth Resources Open File Report 2003-15, 1 sheet, scale 1:100,000. [http://www.dnr.wa.gov/Publications/ger_ofr2003-15_geol_map_shelton_100k.pdf and https://fortress.wa.gov/dnr/geology/?Site=wigm]

Logan, R. L.; Walsh, T. J., 2007, Geologic map of the Vaughn 7.5-minute quadrangle, Pierce and Mason Counties, Washington: Washington Division of Geology and Earth Resources Geologic Map GM-65, 1 sheet, scale 1:24,000. [http://www.dnr.wa.gov/Publications/ger_gm65_geol_map_vaughn_24k.pdf]

Logan, R. L.; Walsh, T. J., 2009, Mima Mounds formation and their implications for climate change [abstract]. *In* Northwest Scientific Association, The Pacific Northwest in a changing environment—Northwest Scientific Association 81st annual meeting; Program with abstracts: Northwest Scientific Association, p. 38-39.

Long, W. A., 1975, Glacial studies on the Olympic Peninsula: U.S. Forest Service, 1 v., 9 plates.

Long, W. A., 1976, Glacial geology of the Olympic Peninsula, Washington: U.S. Forest Service, 135 p.

Magsino, Sammantha; Sanger, Elizabeth; Walsh, T. J.; Palmer, S. P.; Blakely, R. J., 2003, The Olympia structure—Ramp or discontinuity? New gravity data provide more information [abstract]: Geological Society of America Abstracts with Programs, v. 35, no. 6, p. 479.

Mazzotti, Stephane; Dragert, Herb; Hyndman, R. D.; Miller, M. M.; Henton, J. A., 2002, GPS deformation in a region of high crustal seismicity—N. Cascadia forearc: Earth and Planetary Science Letters, v. 198, no. 1-2, p. 41-48, doi:10.1016/S0012-821X(02)00520-4.

McCaffrey, Robert; Qamar, A. I.; King, R. W.; Wells, Ray; Khazaradze, Giorgi; Williams, C. A.; Stevens, C. W.; Vollick, J. J.; Zwick, P. C., 2007, Fault locking, block rotation and crustal deformation in the Pacific Northwest: Geophysical Journal International, v. 169, no. 3, p. 1315-1340.

Molenaar, Dee; Noble, J. B., 1970, Geology and related ground-water occurrence, southeastern Mason County, Washington: Washington Department of Water Resources Water-Supply Bulletin 29, 145 p., 2 plates. [http://www.ecy.wa.gov/programs/eap/wsb/pdfs/WSB_29_Book.pdf and http://www.ecy.wa.gov/programs/eap/wsb/pdfs/ WSB_29_Plates.pdf]

Morrison, Roger B., editor, 1991, Quaternary nonglacial geology--Conterminous U.S.: Geological Society of America DNAG Geology of North America, v. K-2, 672 p., 8 plates in accompanying case.

Mullineaux, D. R.; Gard, L. M., Jr.; Crandell, D. R., 1959, Continental sediments of Miocene age in Puget Sound lowland, Washington: American Association of Petroleum Geologists Bulletin, v. 43, no. 3, pt. 1, p. 688-696.

Naeser, N. D.; Westgate, J. A.; Easterbrook, D. J.; Carson, R. J., 1984, Pre-0.89 my glaciation in the west central Puget Lowland, Washington [abstract]: Geological Society of America Abstracts with Programs, v. 16, no. 5, p. 324.

Nelson, A. R.; Personius, S. F.; Sherrod, B. L.; Buck, Jason; Bradley, Lee-Ann; Henley, Gary, II; Liberty, L. M.; Kelsey, H. M.; Witter, R. C.; Koehler, R. D.; Schermer, E. R.; Nemser, E. S.; Cladouhos, T. T., 2009, Field and laboratory data from an earthquake history study of scarps in the hanging wall of the Tacoma fault, Mason and Pierce Counties, Washington: U.S. Geological Survey Scientific Investigations Map SIM-3060, 3 sheets, scale 1:30,000. [http://pubs.usgs.gov/sim/3060/]

Noble, J. B., 1990, Proposed revision of nomenclature for the Pleistocene stratigraphy of coastal Pierce County, Washington: Washington Division of Geology and Earth Resources Open File Report 90-4, 54 p. [http://www.dnr.wa.gov/publications/ger_ofr90-4_pierce_co_pleistocene_stratigraphy.pdf].

Polenz, Michael; Contreras, T. A.; Czajkowski, J. L.; Legorreta Paulin, Gabriel; Miller, B. A.; Martin, M. E.; Walsh, T. J.; Logan, R. L.; Carson, R. J.; Johnson, C. N.; Skov, R. H.; Mahan, S. A.; Cohan, C. R. 2010b, Supplement to geologic maps of the Lilliwaup, Skokomish Valley, and Union 7.5-minute quadrangles, Mason County, Washington—Geologic setting and development around the Great Bend of Hood Canal: Washington Division of Geology and Earth Resources Open File Report 2010-5, 27 p. [http://www.dnr.wa.gov/Publications/ger_ofr2010-5_lilliwaup_skokomish_valley_union_suppl_24k.pdf]

Polenz, Michael; Czajkowski, J. L.; Legorreta Paulin, Gabriel; Contreras, T. A.; Miller, B. A.; Martin, M. E.; Walsh, T. J.; Logan, R. L.; Carson, R. J.; Johnson, C. N.; Skov, R. H.; Mahan, S. A.; Cohan, C. R., 2010a, Geologic map of the Skokomish Valley and Union 7.5-minute quadrangles, Mason County, Washington: Washington Division of Geology and Earth Resources Open File Report 2010-3, 21 p., 1 plate, scale 1:24,000. [http://www.dnr.wa.gov/Publications/ger_ofr2010-3_geol_map_skokomish_valley_union_24k.zip]

Polenz, Michael; Miller, B. A.; Davies, Nigel; Perry, B. B.; Clark, K. P.; Walsh, T. J.; Carson, R. J.; Hughes, J. F., 2012, Geologic map of the Hoodsport 7.5-minute quadrangle, Mason County, Washington: Washington Division of Geology and Earth Resources Open File Report 2011-3, 1 sheet, scale 1:24,000, 19 p. text. [http://www.dnr.wa.gov/Publications/ger_ofr2011-3_geol_map_hoodsport_24k.zip]

Porter, S. C.; Carson, R. J., 1971, Problems of interpreting radiocarbon dates from dead-ice terrain, with an example from the Puget Lowland of Washington: Quaternary Research, v. 1, no. 3, p. 410-414.

Porter, S. C.; Swanson, T. W., 1998, Radiocarbon age constraints on rates of advance and retreat of the Puget lobe of the Cordilleran ice sheet during the last glaciation: Quaternary Research, v. 50, no. 3, p. 205-213.

Raisz, E. J., 1945, The Olympic–Wallowa lineament: American Journal of Science, v. 243A [Daly volume], p. 479-485.

Reimer, P. J.; Baillie, M. G. L.; Bard, E.; Bayliss, A.; Beck, J. W.; Blackwell, P. G.; Bronk Ramsey, C.; Buck, C. E.; Burr, G. S.; Edwards, R. L.; Friedrich, M.; Grootes, P. M.; Guilderson, T. P.; Hajdas, I.; Heaton, T. J.; Hogg, A. G.; Hughen, K. A.; Kaiser, K. F.; Kromer, B.; McCormac, F. G.; Manning, S. W.; Reimer, R. W.; Richards, D. A.; Southon, J. R.; Talamo, S.; Turney, C. S. M.; van der Plicht, J.; Weyhenmeyer, C. E., 2009, IntCal09 and Marine09 radiocarbon age calibration curves, 0–50,000 years cal BP: Radiocarbon, v. 51, no. 4, p. 1111–1150.

Renne, P. R.; Deino, A. L.; Walter, R. C.; Turrin, B. D.; Swisher III, C. C.; Becker, T. A.; Curtis, G. H.; Sharp, W. D.; Jaouni, A. R., 1994, Intercalibration of astronomical and radioisotopic time: Geology, v. 22, p. 783-786.

Sherrod, B. L., 2001, Evidence for earthquake-induced subsidence about 1100 yr ago in coastal marshes of southern Puget Sound, Washington: Geological Society of America Bulletin, v. 113, no. 10, p. 1299-1311.

Sherrod, B. L.; Brocher, T. M.; Weaver, C. S.; Bucknam, R. C.; Blakely, R. J.; Kelsey, H. M.; Nelson, A. R.; Haugerud, Ralph, 2004, Holocene fault scarps near Tacoma, Washington, USA: Geology, v. 32, no. 1, p. 9-12.

Sherrod, B. L.; Nelson, A. R.; Kelsey, H. M.; Brocher, T. M.; Blakely, R. J.; Weaver, C. S.; Rountree, N. K.; Rhea, B. S.; Jackson, B. S., 2003, The Catfish Lake scarp, Allyn, Washington—Preliminary field data and implications for earthquake hazards posed by the Tacoma fault: Version 1.0: U.S. Geological Survey Open-File Report 03-0455, 1 sheet, with 12 p. text. [http://pubs.usgs.gov/of/2003/of03-455/]

Smith, G. R.; Montgomery, D. R.; Peterson, N. P.; Crowley, Bruce, 2007, Spawning sockeye salmon fossils in Pleistocene lake beds of Skokomish valley, Washington: Quaternary Research, v. 68, no. 2, p. 227-238.

Stuiver, Minze; Polach, H. A., 1977, Discussion: Reporting of ^{14}C Data: Radiocarbon, v. 19, no. 3, 1977.

Stuiver, Minze; Reimer, P. J.; Reimer, R. W., 2010. CALIB 6.0.1 [WWW program and documentation]. Belfast: 14CHRONO Centre, Queen's University Belfast. [Accessed 2010 at http://www.calib.org]

Tabor, R. W.; Cady, W. M., 1978, Geologic map of the Olympic Peninsula, Washington: U.S. Geologic Survey Miscellaneous Investigations Series Map I-994, 2 sheets, scale 1:125,000. [http://ngmdb.usgs.gov/Prodesc/proddesc_9852.htm]

Thorson, R. M., 1981, Isostatic effects of the last glaciation in the Puget Lowland, Washington: U.S. Geological Survey Open-File Report 81-370, 100 p., 1 plate. [http://ngmdb.usgs.gov/Prodesc/proddesc_75484.htm]

Thorson, R. M., 1989, Glacio-isostatic response of the Puget Sound area, Washington: Geological Society of America Bulletin, v. 101, no. 9, p. 1163-1174.

Walker, J. D.; Cohen, H. A., compilers, 2006, AGI data sheets—The geoscience handbook; 4th ed.: American Geological Institute, 302 p.

Walsh, T. J.; Logan, R. L., 2007, Field data for a trench on the Canyon River fault, southeast Olympic Mountains, Washington: Washington Division of Geology and Earth Resources Open File Report 2007-1, 1 plate. [http://www.dnr.wa.gov/Publications/ger_ofr2007-1_canyon_river_fault_trench.pdf]

Walsh, T. J.; Logan, R. L.; Polenz, Michael; Schasse, H. W., 2003, Geologic map of the Nisqually 7.5-minute quadrangle, Thurston and Pierce Counties, Washington: Washington Division of Geology and Earth Resources Open File Report 2003-10, 1 sheet, scale 1:24,000. [http://www.dnr.wa.gov/Publications/ger_ofr2003-10_geol_map_nisqually_24k.pdf]

Wells, R. E.; Weaver, C. S.; Blakely, R. J., 1998, Fore-arc migration in Cascadia and its neotectonic significance: Geology, v. 26, no. 8, p. 759-762.

Westgate, J. A.; Easterbrook, D. J.; Naeser, N. D.; Carson, R. J., 1987, Lake Tapps tephra—An early Pleistocene stratigraphic marker in the Puget Lowland, Washington: Quaternary Research, v. 28, no. 3, p. 340-355.

Wilson, J. R., 1975, Geology of the Price Lake area, Mason County, Washington: North Carolina State University Master of Science thesis, 79 p., 2 plates.

Wilson, J. R.; Bartholomew, M. J.; Carson, R. J., 1979, Late Quaternary faults and their relationship to tectonism in the Olympic Peninsula, Washington: Geology, v. 7, no. 5, p. 235-239.

Witter, R. C.; Givler, R. W., 2005, Two post-glacial earthquakes on the Saddle Mountain west fault, southeastern Olympic Peninsula, Washington—Final technical report. U.S. Geological Survey Earthquake Hazards Program, External Research Support, Funded Research Final Technical Reports, 50 p. [http://earthquake.usgs.gov/research/external/reports/05HQGR0089.pdf]

Witter, R. C.; Givler, R. W.; Carson, R. J., 2008, Two post-glacial earthquakes on the Saddle Mountain west fault, southeastern Olympic Peninsula, Washington: Bulletin of the Seismological Society of America, v. 98, no. 6, p. 2894-2917.

Yount, J. C.; Dembroff, G. R.; Barats, G. M., 1985, Map showing depth to bedrock in the Seattle 30' by 60' quadrangle, Washington: U.S. Geological Survey Miscellaneous Field Studies Map MF-1692, 1 sheet, scale 1:100,000.

Zdanowicz, C. M.; Zielinski, G. A.; Germani, M. S., 1999, Mount Mazama eruption—Calendrical age verified and atmospheric impact assessed: Geology, v. 27, no. 7, p. 621-624.

Appendix A. Age-control data

Age-control data from the map area (and a fault investigation trench 1,500 ft west of the map area): Age sample sites are those shown in Polenz and others (2012). Uncertainty values preceded by "±" are one standard deviation (68% confidence interval) and age ranges reported as "number-to-number" span two standard deviations (2σ = 95% confidence interval); uncertainty statements from other studies are shown in quotation marks if we are unsure of their meaning. Radiocarbon "greater than" age statements (for example, >43,500 B.P.) include a 2σ variance against background radiation. Uncertainty statements reflect random and lab errors; errors from unrecognized sample characteristics or flawed methodological assumptions (for example, ^{14}C sample contamination from younger carbon flux) are not known. ^{14}C, radiocarbon analysis; AMS, radiocarbon analysis by atomic mass spectrometry; "^{14}C" includes instances where referenced sources did not specify if analysis was AMS or conventional. One-sigma ^{14}C age estimates (including AMS) are either in radiocarbon years before 1950 (^{14}C yr. B.P.) or, where displayed in "quotation marks", as reported by prior publication; ^{14}C ages stated in ka are in calendar years before 1950. One-sigma ^{14}C ages (including AMS) are "conventional" (adjusted for measured $^{13}C/^{12}C$ ratio) if a $^{13}C/^{12}C$ ratio is shown; other entries may be "measured" or "conventional". Geologic units are the interpretation of this study for the sample host material, and for subsurface samples, these may differ from map units. Elevations are in feet (estimated by us using Puget Sound Lidar Consortium lidar grid elevations projected to State Plane South, NAD 83 HARN, US Survey feet, supplemented by visual elevation estimates on bluffs. Lidar elevation statements were not adjusted to account for systematic projection differences relative to base map). Latitude and longitude coordinates generated from sample locations as plotted in ArcGIS (projection State Plane South, NAD 83 HARN, US Survey ft).

Age sample site	Age sample ID	Site name	Age estimate (^{14}C yr B.P. or ka or Ma)	Analytical method	$^{13}C/^{12}C$ (o/oo)	Material dated	Geologic unit	Lab or lab no.*	Elev. (ft)	Reference	Original sample ID	Notes	Lat/Long
SMWT 2	SMWT 2a	Saddle Mtn West fault trench 2 (Cargill Creek)	1,020 ±35 B.P. (1.050-0.800 ka)	AMS	-25.1	detrital charcoal	Qaf	GX 32081	~763	Witter and others (2008); Rob Witter, written commun., 2010	PL05 RC-10	Sample from colluvium	47.46595/ -123.18162
H1	H1a	Price Lake – Hughes 1	1,050 ±30 B.P. (1.050-0.920 ka)	AMS	-29.08	wood	Qp	NOS AMS OS-46780	<720	Jonathan Hughes, unpublished$	PLC4 D1-79	Soil beneath lake deposits, 0-2 cm beneath earthquake contact (i.e., contact formed by sediment deposition atop a former surface that was subjected to a land level change during an earthquake and consequently ended up in a depositional environment—in this case a lake floor); wood sampled may have rested on top of buried soil; twigs have pith and bark; maximum age estimate for a Saddle Mountain East fault earthquake	47.47001/ -123.17142
H2	H2a	Price Lake – Hughes 2	1,150 ±40 B.P. (1.170-0.970 ka)	AMS	-29.9	Western hemlock (*Tsuga heterophylla*) needles	Qp	Beta-204316	<723	Jonathan Hughes, unpublished$	PLDRU M 8	Soil beneath wetland deposits, sampled just below earthquake contact; maximum limiting age estimate for a Saddle Mountain East fault earthquake	47.47014/ -123.16809
SMEP	SMEP	pond northeast of Saddle Mountain	1,155 ±85 B.P.	^{14}C		submerged wood	Qp (stump in pond)	I-7557?^	~817	Wilson (1975); Wilson and others (1979)	I-7557	Stump in pond northeast of Saddle Mountain. Location approximate; date thought to approximate an event on the Saddle Mountain East fault	47.48/ -123.15

H3	H3a1	Price Lake – Hughes 3	1,210 ±35 B.P. (1.260-1.060 ka)	AMS	-25.97	Western redcedar (*Thuja plicata*) cone	Qp	NOS AMS OS-46846	725	Jonathan Hughes, unpublished$	PLTA 20-63	Putative A horizon of buried soil beneath wetland deposits, just beneath earthquake contact (61 cm); sample depth 63-65 cm; overlies charcoal horizon of sample H3a2; may have washed in after earthquake?; maximum limiting age estimate for a Saddle Mountain East fault earthquake	47.46810/ -123.17076
H4	H4	Price Lake – Hughes 4	1,210 ±40 B.P. (1.260-1.010 ka)	AMS	-30	Western hemlock (*Tsuga heterophylla*) needles	Qaf	Beta-193648	<716	Jonathan Hughes, unpublished$	PLC1 D3-2	Soil beneath lake deposits, 2-3 cm beneath putative earthquake contact; 202-203 cm depth; maximum limiting age estimate for a Saddle Mountain West fault earthquake.	47.47304/ -123.17235
H5	H5a	Price Lake – Hughes 5	1,220 ±40 B.P. (1.270-1.060 ka)	AMS	-22.5	Douglas fir (*Pseudotsuga menziesii*) wood; same submerged stump as PL357EX	Qaf (stump sticks up into water)	Beta-212219	<723	Jonathan Hughes, unpublished$	PL 357IN	Top of same in situ submerged tree stump as sample H5b; outer growth rings lost to weathering; maximum limiting age estimate for a Saddle Mountain West fault earthquake; anticipated age greater than that of H5b, but the two age estimates are statistically identical	47.47382/ -123.17263
H6	H6a1	Price Lake – Hughes 6	1,230 ±40 B.P. (1.270-1.060 ka)	AMS	-21.61	leaves of wetland plants; some may be cranberry (*Vaccinium oxycoccos*)	Qp	NOS AMS OS-47168	720	Jonathan Hughes, unpublished$	PLTC 50-85-87	Top of buried soil; sample matrix included some aquatic [seeds?] and gyttja suggesting disturbance at contact; sample depth 87-89 cm; maximum limiting age estimate for a Saddle Mountain East fault earthquake	47.46918/ -123.17074
H3	H3b1	Price Lake – Hughes 7	1,240 ±30 B.P. (1.270-1.080 ka)	AMS	-26.76	wetland seed mix	Qp	NOS AMS OS-46847	724	Jonathan Hughes, unpublished$	PLTA 27.5-63	Lake or wetland deposit directly overlying earthquake contact; sample depth 63-65 cm; minimum limiting age estimate for a Saddle Mountain East fault earthquake	47.46815/ -123.17082
H8	H8	Price Lake – Hughes 8	1,240 ±35 B.P. (1.270-1.070 ka)	AMS	-28.3	wood	Qoa or Qgt	NOSAMS OS-46983	<719	Jonathan Hughes, unpublished$	PLC2 D2-125	Soil beneath lake deposits; top of buried soil, beneath earthquake contact; two pieces of wood (twigs) submitted, bark on both; 125-127 cm; maximum limiting age estimate for a Saddle Mountain East fault earthquake	47.47111/ -123.16889
H3	H3b2	Price Lake – Hughes 7	1,250 30 B.P. (1.270-1.080 ka)	AMS	-25.69	Western redcedar (*Thuja plicata*) cone	Qp	NOS AMS OS-47272	724	Jonathan Hughes, unpublished$	PLTA 27.5-65	Soil beneath wetland deposits, sampled at top of earthquake contact; sample depth 65-67 cm; maximum limiting age estimate for a Saddle Mountain East fault earthquake	47.46815/ -123.17082
H5	H5b	Price Lake – Hughes 5	1,250 ±40 B.P. (1.280-1.080 ka)	AMS	-21.2	Douglas fir (*Pseudotsuga menziesii*) wood; same stump as PL357IN	Qaf (stump sticks up into water)	Beta-212218	<723	Jonathan Hughes, unpublished$	PL357EX	Top of same in situ submerged tree stump as sample H5a; outer growth rings lost to weathering; maximum limiting age estimate for a Saddle Mountain West fault earthquake; anticipated age less than that of H5a, but the two age estimates are statistically identical	47.47382/ -123.17263

Age sample site	Age sample ID	Site name	Age estimate (^{14}C yr B.P. or ka or Ma)	Analytical method	^{13}C/^{12}C (o/oo)	Material dated	Geologic unit	Lab or lab no.*	Elev. (ft)	Reference	Original sample ID	Notes	Lat/Long
H9	H9	Price Lake – Hughes 9	1,270 ±40 B.P. (1.290-1.080 ka)	AMS	-27.8	Western hemlock (*Tsuga heterophylla*) needles	Qoa or Qgt	Beta-193649	<720	Jonathan Hughes, unpublished$	PLC3 D1-88-89	Soil beneath lake deposits, beneath earthquake contact; 88-89.5 cm depth; maximum limiting age estimate for a Saddle Mountain East fault earthquake	47.47074/ -123.16756
PLW1	PLW1	Price Lake (Wilson)	1,315 ±80 B.P.	^{14}C		submerged wood	Qp (stump beneath water)	I -7757?^	~712	Wilson (1975); Wilson and others (1979)	I-7757	Stump submerged in Price Lake (11 ft water depth), drowned by east-up surface offset on the Saddle Mountain East fault; location approximate	47.47/ -123.17
AT	AT02	Alligator Trench (Dow Mountain)	1,360 ±40 B.P. (1.340-1.180 ka#)	AMS	-25.9	charcoal	Qmw	Beta-264361	~1387	Barnett and others (2009b); Elizabeth Barnett, written commun., 2010	AT-02	Buried soil within colluvium. 1,260-1,330 B.P.; site mapped as Crescent basalt because regolith is too thin to map as surface geology unit	47.46047/ -123.15782
SMWT 2	SMWT 2b	Saddle Mtn West fault trench 2 (Cargill Creek)	1,390 ±50 B.P. (1.390-1.180 ka)	AMS	-22.7	detrital charcoal	Qaf	GX 32079	~763	Witter and others (2008); Rob Witter, written commun., 2010	PL05 RC-4	Sample from colluvium	47.46595/ -123.18162
H6	H6b	Price Lake – Hughes 10	1,490 ±40 B.P. (1.510-1.300 ka)	AMS	-26.3	Western white pine (*Pinus monticola*) fascicle and needle bases	Qp	Beta-194761	722	Jonathan Hughes, unpublished$	PLTC 80-77	Soil beneath wetland deposits, sampled just below earthquake contact; sample depth 77.5-78.5 cm; maximum limiting age estimate for a Saddle Mountain East fault earthquake	47.46892/ -123.17063
H2	H2b	Price Lake – Hughes 11	1,510 ±40 B.P. (1.520-1.310 ka)	AMS	-25.1	detrital charcoal	Qp	Beta-204315	719	Jonathan Hughes, unpublished$	PLDRUM 6	Soil? beneath wetland deposits, picked from horizon beneath putative earthquake contact (gyttja over paleosol?); sample associated with charcoal stained deposit; sample depth 124-129 cm; core suggests two submergence events due to Saddle Mountain East fault rupture, and if so, this sample is a maximum limiting age estimate for the older event	47.47013/ -123.16785
SMWT 2	SMWT 2c	Saddle Mtn West fault trench 2 (Cargill Creek)	1,550 ±40 B.P. (1.530-1.360 ka)	AMS	-26.1	detrital charcoal	Qaf	GX 32082	~763	Witter and others (2008); Rob Witter, written commun., 2010	PL05 RC-15	Sample from colluvium	47.46595/ -123.18162
SMET 1	SMET 1a	Saddle Mtn East fault trench 1	1,600 ±200 B.P.	^{14}C		charcoal	Qmw	W 3031?^	~1114	Wilson (1975); Wilson and others (1979)	W-3031	Charcoal sample from colluvium on downthrown (west) side of fault	47.48093/ -123.15527

SMET 1	SMET 1b	Saddle Mtn East fault trench 1	1,750 ±40 B.P. (1.810-1.550 ka#)	AMS	-24.5	detrital charcoal	Qgic	Beta-264364	~1113	Barnett and others (2009b); Elizabeth Barnett, written commun., 2010	LS-04	Charcoal in cobbly, pebbly, loamy sand soil of apparent Vashon Stade glacial parent material, on downthrown (west) side of fault	47.48093/ -123.15527
SMWT 2	SMWT 2d	Saddle Mtn West fault trench 2 (Cargill Creek)	1,760 ±40 B.P. (1.810-1.560 ka)	AMS	-26.7	detrital charcoal	Qaf	GX 32080	~763	Witter and others (2008); Rob Witter, written commun., 2010	PL05 RC-6	Sample from colluvium	47.46595/ -123.18162
SMWT 2	SMWT 2e	Saddle Mtn West fault trench 2 (Cargill Creek)	1,820 ±35 B.P. (1.860-1.630 ka)	AMS	-23.1	detrital charcoal	Qaf	GX 32084	~763	Witter and others (2008); Rob Witter, written commun., 2010	PL05 RC-18	Sample from colluvium	47.46595/ -123.18162
H3	H3a2	Price Lake – Hughes 3	1,890 ±30 B.P. (1.900-1.730 ka)	AMS	-22.21	detrital charcoal	Qp	NOS AMS OS-47102	725	Jonathan Hughes, unpublished$	PLTA 20-65	Soil beneath wetland deposits; sampled in top 2 cm of charcoal horizon that is 5 cm beneath putative earthquake contact; sample depth 65-67 cm; maximum limiting age estimate for a Saddle Mountain East fault earthquake	47.46810/ -123.17076
H1	H1b	Price Lake – Hughes 1	3,000 ±30 B.P. (3.320-3.080 ka)	AMS	-26.58	Western redcedar (*Thuja plicata*) scales	Qp	NOS AMS OS-46982	<718	Jonathan Hughes, unpublished$	PLC4 D2-147	Soil? beneath lake deposits, just beneath a contact that appears to be soil overlain by gyttja; organics dated are from top 2 cm of buried soil; more than two dozen scales collected; lots of herbaceous material and little wood in deposit; 147-149 cm depth; maximum limiting age estimate for whatever the contact represents; subsidence would appear to be tied to the Saddle Mountain East fault	47.47001/ -123.17142
AT	AT13	Alligator Trench (Dow Mountain)	3,370 ±40 B.P. (3.700-3.480 ka#)	AMS	-24.4	charcoal	Qmw	Beta-264362	~1387	Barnett and others (2009b); Elizabeth Barnett, written commun., 2010	AT-13	Sampled from abundant charcoal atop former denudation surface, overlain by colluvium and overlying lodgement till; site mapped as Crescent basalt because regolith is too thin to map as surface geology unit	47.46047/ -123.15782

Age sample site	Age sample ID	Site name	Age estimate (^{14}C yr B.P. or ka or Ma)	Analytical method	^{13}C/^{12}C (o/oo)	Material dated	Geologic unit	Lab or lab no.*	Elev. (ft)	Reference	Original sample ID	Notes	Lat/Long
Qoa	Qoa3	Price Lake east drainage, upper terrace	4,700 ±40 B.P. (5.590-5.310 ka)	AMS	-24.4	detrital charcoal	Qoa	Beta-194797	~725	Jonathan Hughes, unpublished$	PLTER 2A-2	Sample represents base of wetland deposits atop the second-lowermost relict fluvial terrace above the modern flood plain associated with Price Lake outlet (east of the Saddle Mountain East fault); sample age was thus expected to exceed those of Qoa1 and Qoa2; the fact that it did not suggests a post-fire pulse of geomorphic activity followed by minimal geomorphic modification during the past 6,000 years; the age need not be associated with an earthquake but may be associated with a fire	47.47379/ -123.15605
SMET 1	SMET 1c	Saddle Mtn East fault trench 1	4860 ±40 B.P. (5.660-5.480 ka#)	AMS	-24.1	detrital charcoal	Qgic	Beta-264363	~1113	Barnett and others (2009b); Elizabeth Barnett, written commun., 2010	LS-03	Charcoal in cobbly, pebbly, loamy sand soil of apparent Vashon Stade glacial parent material, on downthrown (west) side of fault	47.48093/ -123.15527
Qoa	Qoa1	Price Lake, east drainage channel margin	5,070 ±40 B.P. (5.920-5.720 ka)	AMS	-24.6	detrital charcoal	Qoa	Beta-194760	~710	Jonathan Hughes, unpublished$	PLS04	Charcoal extracted from creek bank beneath modern flood plain terrace (east of the Saddle Mountain East fault); age was expected to be the most recent of terrace ages but is equal to Qoa2 and older than Qoa3, suggesting a post-fire pulse of geomorphic activity followed by minimal geomorphic modification during the past 6,000 years; the age need not be associated with an earthquake	47.47379/ -123.15605
Qoa	Qoa2	Price Lake, east drainage lower terrace	5,080 ±40 B.P. (5.920-5.730 ka)	AMS	-26.2	detrital charcoal	Qoa	Beta-194759	~720	Jonathan Hughes, unpublished$	PLTER 1A-1	Sample represents base of wetland deposits atop the lowermost relict fluvial terrace above the modern flood plain associated with Price Lake outlet (east of the Saddle Mountain East fault); given that the age here is unexpectedly younger than for Qoa3 and the same as for charcoal extracted from the creek bank (Qoa1), the age need not be associated with a past earthquake but seems to mark a post-fire pulse of geomorphic activity followed by minimal geomorphic activity during the past 6,000 years	47.47379/ -123.15605

PLW2	PLW2	Price Lake (Wilson)	5,100 ±500 B.P.	^{14}C		submerged wood	Qp (stump beneath water)		~713	Wilson (1975); Wilson and others (1979)	WW-60	Sample from stump submerged in Price Lake (10 ft water depth), drowned by east-up surface offset on the Saddle Mountain East fault; approximately located; Wilson and others (1979) note that analytical problems render the age questionable	47.47/ -123.17
H1	H1c	Price Lake – Hughes 1	5,830 ±45 B.P. (6.740-6.500 ka)	AMS	-27.17	wood	Qp	NOS AMS OS-46781	<714	Jonathan Hughes, unpublished$	PLC4 D3-262	Soil? beneath lake deposits; sample from 2-3 cm beneath woody horizon (dated) overlain by non-woody horizon that is slightly lighter in color; pith present; bark removed before submitting sample; twig found at contact between 263 and 264 cm depth; maximum limiting age estimate for whatever the contact represents; subsidence would appear to be tied to the Saddle Mountain East fault	47.47001/ -123.17142
SMWC	SMWC1	Saddle Mtn West fault core transect	7,380 ±50 B.P. (8.330-8.040 ka)	^{14}C	-30	peat	Qp	GX 32248	~729	Witter and others (2008); Rob Witter, written commun., 2010	PL05 C1	Saddle Mountain West fault sediment core transect (NW-SE) 330 ft southwest of Price Lake, buried peat 8.5 ft below surface, from fault riser slope, and southeast of sample SMWC2	47.46852/ -123.17790
SMWT 2	SMWT 2f	Saddle Mtn West fault trench 2 (Cargill Creek)	7,650 ±50 B.P. (8.540-8.380 ka)	AMS	-23.1	detrital charcoal	Qaf	GX 32083	~763	Witter and others (2008); Rob Witter, written commun., 2010	PL05 RC-16	Sample from colluvium	47.46595/ -123.18162
SMWC	SMWC 2	Saddle Mtn West fault core transect	7,720 ±50 B.P. (8.590-8.420 ka)	^{14}C	-27.8	detrital seeds sampled from peat	Qp	GX 32249	~729	Witter and others (2008); Rob Witter, written commun., 2010	PL05 D3	Saddle Mountain West fault sediment core transect (NW-SE) 330 ft southwest of Price Lake, seeds from buried peat 11 ft below surface, from northwest (down) side of fault, and northwest of sample SMWC1	47.46860/ -123.17803
H6	H6a2	Price Lake – Hughes 6	8,080 ±45 B.P. (9.130-8.780 ka)	AMS	-26.66	herbaceous floral parts; fruit wall and subtending bristles	Qp	NOS AMS OS-46986	715	Jonathan Hughes, unpublished$	PLTC 50-246	Horizon sampled (buried soil?) lies beneath a complex transition from soil to gyttja (gyttja over soil); sampled 6 cm beneath contact; sample depth 246-248 cm; maximum limiting age estimate for whatever the contact represents; subsidence would appear to be tied to the Saddle Mountain East fault	47.46918/ -123.17074

Age sample site	Age sample ID	Site name	Age estimate (^{14}C yr B.P. or ka or Ma)	Analytical method	^{13}C/^{12}C (o/oo)	Material dated	Geologic unit	Lab or lab no.*	Elev. (ft)	Reference	Original sample ID	Notes	Lat/Long
SLS	SLS	Southern Lilliwaup Swamp	8,715 ±185 B.P.	^{14}C		wood	Qp	I 8174?^	~768	Wilson (1975); Wilson and others (1979)	I-8174	Sample from buried organic layer in Lilliwaup Swamp; sample location approximate and based on Wilson (1975); Wilson and others (1979) label the date a "questionable" age estimate for a Saddle Mountain West fault event	47.49/ -123.17
UFCVA	UFCVA	Upper Finch Creek Vashon Advance	13,410 ±80 B.P. (16.140-15.690 ka)	^{14}C	-30.5	detrital plant fragments and peat	Qga	Beta-288370	~550	This report	10-76-M-1189	Rare cluster of detrital small sticks, peat, and soft plant debris from laminated to structureless silt and clay in an ice-dammed, local lake section consisting of alternating Vashon advance outwash gravel and lacustrine fines; date marks arrival of Vashon ice (see text on timing and duration of Vashon ice); lab reports 2-sigma calendric age as 14,190 to 13,740 B.C.	47.41813/ -123.15421
SCVA	SCVA	Sund Creek Vashon Advance	14,130 ±60 B.P. (17.010-16.700 ka)	AMS	-26.5	detrital wood fragments	Qga	Beta-288369	~1072	This report	10-68-M-1007	Rare, small cluster of detrital wood (from small sticks) in laminated to structureless silt and clay in an ice-dammed, local lake section consisting of alternating Vashon advance outwash gravel and lacustrine fines; date marks arrival of Vashon ice (see text on timing and duration of Vashon ice); lab reports 2-sigma calendric age as 15,060 to 14,750 B.C.	47.45058/ -123.15421
FCP	FCP	Frigid Creek peat	>41,000 B.P.	^{14}C		peat	Qpl	W 3030	~421	Birdseye and Carson, 1989; Carson, 1980; Robert Carson, written commun., 2010	W-3030	Sample W3030 (Carson, 1980) from 3 ft-thick, massive gray clay with 2 in.-thick peat layers in small, unnamed tributary on south valley wall of Frigid Creek, 60 ft upsection from 900 ka "Frigid Creek tephra" (see below); intervening section lacks obvious disconformity; lab no. suggests ^{14}C analysis by USGS National center, and John Sims of the USGS visited the site and may have gotten a date	47.37599/ -123.24491
MTCD	MTCD	McTaggert Creek diamicton	>43,500 B.P.	^{14}C	-27.9	detritus from small sticks	Qapd	Beta-289586	~549	This report	10-13-M-185	Small, detrital sticks in sandy diamicton (paleosol or debris flow deposit), overlain by Olympic source, pre-Fraser gravel	47.39607/ -123.23176

LFC	LFC	Lower Finch Creek	>46,290 B.P.	^{14}C	-26.3	coniferous wood	Qapd	Beta-288371	~340	This report	10-76-M-1202	Two ft-wide, flattened log from 5 ft section of gray, laminated clay (with other small wood debris), overlain by 4 ft sandy cobble gravel and underlain by 2 ft bedded sand, all from within a 100 ft section of clayey, sandy gravel with sand lenses; wood was identified as coniferous by Kathleen Hawes, South Puget Sound Community College, and approximates apparent transition from unit Qapd (downsection) to Qpo (upsection)	47.41044/ -123.24413
FCT	FCT	Frigid Creek tephra	900 ±150 ka	fission track		tephra (glass)	Qpl		~360	Naeser and others, 1984; Westgate and others, 1987	UT-55	Fission track age on glass (not zircon) in tephra sample UT 55 from small, unnamed tributary on south valley wall of Frigid Creek (base of a couplet of fining-up tephra layers, bracketed by magnetically reversed lake beds); first published in Naeser and others (1984), more detail provided in Westgate and others (1987)	47.37616/ -123.24413
CHU	CHU	Cushman Hill Upper	36.18 ±0.46 Ma	^{40}Ar-^{39}Ar		basalt (flow)	Ev_c	Noble Gas Mass Spectro-metry Lab, Oregon State Univ.	1485	This report	10-54-M-851-b	Basalt from 30 ft-thick flow; chemistry (Table 1) and location suggest Upper Crescent Fm association, but the late Eocene age estimate is unexpectedly young for Crescent Fm; lab reports unusually large step age uncertainties (0.48%) due to low K_2O content but also notes a good plateau age@, with no evidence for diffusion loss (only low-temperature weathering of groundmass to clays/ zeolites); for full analytical results of the $^{40}Ar/^{39}Ar$ analysis, contact the Washington Division of Geology and Earth Resources	47.44172/ -123.23987
SHADING BELOW IDENTIFIES AGE-CONTROL DATA FROM OUTSIDE THE HOODSPORT 7.5-MINUTE QUADRANGLE													
	HB-018	Frigid Creek fault trench (1,500 ft west of map area)	415 ±40 B.P. (0.526-0.319 ka)	AMS	-25&	charcoal	Qgta?	CAMS 101673	~737	Blakely and others (2009a); Brian Sherrod, written commun., 2011	HB-018	Interface between surficial sandy gravel and underlying colluvium that Blakely and others (2009a) interpreted as fault-offset-related; sampled 2003 by Shasta Sherrod and Brian Sherrod (U.S. Geological Survey)	47.393/ -123.257
	HB-013	Frigid Creek fault trench (1,500 ft west of map area)	3,925 ±40 B.P. (4.513-4.220 ka)	AMS	-25&	charcoal	Qgta?	CAMS 101671	~739	Blakely and others (2009a); Brian Sherrod, written commun., 2011	HB-013	Sandy silt, interpreted by Blakely and others (2009a) as buried soil; sampled 2003 by Shasta Sherrod and Brian Sherrod (U.S. Geological Survey)	47.393/ -123.257

Age sample site	Age sample ID	Site name	Age estimate (^{14}C yr B.P. or ka or Ma)	Analytical method	^{13}C/^{12}C (o/oo)	Material dated	Geologic unit	Lab or lab no.*	Elev. (ft)	Reference	Original sample ID	Notes	Lat/Long
	HB-015	Frigid Creek fault trench (1,500 ft west of map area)	3,990 ±40 B.P.	AMS	-25&	charcoal	Qgta?	CAMS 101672	~739	Blakely and others (2009a); Brian Sherrod, written commun., 2011	HB-015	Sandy silt, interpreted by Blakely and others (2009a) as buried soil. Sampled 2003 by Shasta Sherrod and Brian Sherrod (U.S. Geological Survey).	47.393/ -123.257
	HB-012	Frigid Creek fault trench (1,500 ft west of map area)	3,990 ±40 B.P.	AMS	-25&	charcoal	Qgta?	CAMS 101670	~732	Blakely and others (2009a); Brian Sherrod, written commun., 2011	HB-012	Sandy loam, interpreted by Blakely and others (2009a) as buried soil. Sampled 2003 by Shasta Sherrod and Brian Sherrod (U.S. Geological Survey).	47.393/ -123.257
	HB-002	Frigid Creek fault trench (1,500 ft west of map area)	4,850 ±40 B.P. (5.657-5.476 ka)	AMS	-25&	charcoal	Qgta?	CAMS 101669	~732	Blakely and others (2009a); Brian Sherrod, written commun., 2011	HB-002	Sandy silt, interpreted by Blakely and others (2009a) as buried soil. Sampled 2003 by Shasta Sherrod and Brian Sherrod (U.S. Geological Survey).	47.393/ -123.257

* Letter combinations within lab numbers shown identify radiocarbon lab codes. Institutions associated with each lab code are: GX, Geochron Laboratories; NOSAMS OS, National Ocean Sciences Accelerator Mass Spectrometry Facility; Beta, Beta Analytic; I, Teledyne Isotopes; W, U.S. Geological Survey, National Center; CAMS, Center for Accelerator Mass Spectrometry, Lawrence Livermore National Laboratory.

Two-sigma age range (ka) was computed by Elizabeth Barnett using Calib 2009 (Stuiver and others, 2010) with reference to the calibration curve intcal09.14c (Reimer and others, 2009) and therefore differs from the age range earlier stated in lab report (Barnett and others, 2009b) and for samples AT02 and AT13 (Czajkowski and others, 2009b).

^ Radiocarbon laboratory inferred from sample number and lab code list at http://www.radiocarbon.org/Info/labcodes.html. Lab report or other corroborating evidence not located for sample.

& ^{13}C/^{12}C ratio assumed according to Stuiver and Polach (1977)

$ Sample from Jonathan Hughes, dated as part of a U.S. Geological Survey–sponsored Mendenhall Fellowship. Interpretation of the Price Lake area work from that fellowship were presented by Hughes (2005), but most details of individual samples and their analyses are first published herein.

@ Plateau age calculated using 10 (of a total 12) heating steps; these 10 steps represent 89.6% of the sample's ^{39}Ar release. Lab comments that the "clear ten-step plateau age can be interpreted simple [*sic*] as crystallization age". Sample irradiated 6 hours at 1 MW power at Oregon State University TRIGA reactor, 31 March 2011. Lab used FCT-3 biotite known 28 ±0.18 Ma age standard (Renne and others, 1994). Lab methods similar to those described by Koppers and others (2003).